Neogene–Quaternary Initiation of the Southern Malawi Rift linked to Reactivation of the Carboniferous–Jurassic Shire Rift

Oyewande Ojo[1], Stuart N. Thomson[2], and Daniel A. Laó-Dávila[1]

[1]Boone Pickens School of Geology, Oklahoma State University

[2]Department of Geosciences, University of Arizona

Corresponding author: Oyewande Ojo (oyewande.ojo@okstate.edu)

Key Points:

- Miocene-Pliocene onset of rifting along the Southern Malawi Rift and linkage to reactivation of the older Shire Rift to its south
- Onset of Cenozoic rifting coeval along the full length of Malawi Rift
- Cooling ages and thermal episodes constrained by apatite fission-track analysis
- Lower extension rates southward along the Malawi Rift
- High fault density suggests linkage between the Malawi Rift and the reactivated Shire Rift

Abstract

Low-temperature thermochronology studies record Miocene aged rift initiation of the northern Malawi Rift. However, no studies are available from the southern Malawi Rift and the Shire Rift, which are thought to have initiated at a later time. Here we present thermal history models derived from new apatite fission-track and (U-Th)/He data from the footwalls of major border faults of the southern Malawi Rift, that reveal three distinct cooling episodes in the Cretaceous, Eocene–Oligocene, and Late Oligocene–Pliocene. These results suggest that the southern Malawi Rift has been accommodating strain along its border faults since the Miocene, just as in the northern Malawi Rift. The timing and rate of extensional strain was further constrained through the application of remote sensing. These results, when combined with our thermal history modeling, yield inferred deformation strain rates that support linkage between the modern Malawi Rift and the older Shire Rift. Cooling histories show that the border faults of the southern Malawi Rift have likely been active since the Late Oligocene - Early Miocene and that this activity has caused linkage and transfer of strain to the older Shire Rift which our results suggest to have been reactivated since the Miocene too. These results provide evidence of the coeval onset of extension along the full length of Malawi Rift and possibly the Western Branch of the East African Rift System.

1 Introduction

The Malawi Rift, which forms the southernmost part of the Western Branch of the East African Rift System, is an early-stage magma-poor continental rift that trends N-S and seems to terminate to the south at the NW-SE trending Shire GrabenRift (Figure 1). The Shire Rift is considered a Paleozoic-Mesozoic rift based on the age of the sedimentary rocks in the rift basin (Castaing, 1991; Figure 2). However, the steep scarps of the Thyolo Fault, a border fault segment of the Shire Rift, and recent earthquakes along strike (e.g., 2007 M4.8 earthquake) suggest that the rift has been reactivated. However, how the Malawi Rift has developed over time, and the evolution of strain accommodation and linkage between the two rifts remains poorly understood, and a matter of debate.

Previous studies show that the evolution of faulting along continental rifts can be inferred from a series of structural and tectonic attributes along the rift (Bonini et al., 2005). These attributes include the direction of younging of the border faults (Abbate and Sagri, 1980; WoldeGabriel et al., 1990, 2016), the increase in the elastic thickness of the lithosphere and border fault length (Hayward and Ebinger, 1996), increase in delay times between the fast and slow S waves correlating with an increase in strain and with lower crustal residence times for erupted lavas (Furman et al., 2004; Maguire et al., 2003), migration of the volcanism from the region (Zanettin et al., 1980), and deepening of mantle intrusion below the rift axis and higher alkalinity of basalts (Mahatsente et al., 1999).

Strain accommodation along rift systems is typically characterized by uplift, erosion, exhumation, and subsidence. The rocks within uplifted major normal fault footwall blocks tend to cool down, either as a result of direct tectonic uncovering by removal of the hanging wall or by erosional exhumation of the uplifted fault block. Meanwhile, the rocks within the subsided hanging wall block within the rift basin itself are usually heated due to burial under sediment and/or enhanced heat flow within the rift (Ehlers et al., 2001; Stockli, 2005). The amount of fault slip accumulated may therefore be recorded by the difference in the thermal signature between rocks across the fault boundary, or by the cooling history of the footwall block itself. The difference in the thermal signature may become large enough to be resolved by low-temperature thermochronometry and thus be used to place constraints on the timing and magnitude of vertical components of the accumulated fault motions (Ehlers et al., 2001; Stockli et al., 2005). Although there are some known ages for the onset of rifting from low-temperature thermochronological studies along the Livingstone Fault in the northern Malawi Rift (Van der Beek et al., 1998; Mortimer et al., 2016), and cooling of the Chilwa Alkaline Province in southern Malawi (Eby et al., 1995), there remains a data gap to constrain ages of onset of strain accommodation and transfer along the main border faults of the southern Malawi Rift and Shire Rift. Moreover, there is a lack of imaging of upper crustal structures in the transfer zone of these two rifts. Thus, we do not know how strain is being accommodated nor the linkage between these two rift basins with different tectonic histories and orientations.

This study focuses on the southern part of the Malawi Rift and the northern part of the Shire Rift and intends to answer the following questions: 1) when did Cenozoic Rifting begin in the southern Malawi Rift? and 2) is there Cenozoic rifting in the Shire Rift? Furthermore, we aim to test whether: 1) The initiation of rifting in the southern Malawi Rift is relatively younger than the northern Malawi Rift (Castaing et al., 1991; Daszinnies et al., 2008), and 2) The geometry of the Southern Malawi Rift and Paleozoic-Mesozoic Shire Rift at the transfer zone indicates strain is being accommodated by rift linkage of isolated and distributed faults; hence whether there is evidence of Cenozoic rifting and reactivation of the Shire Rift.

To achieve these aims, this study presents new apatite fission track and (U-Th)/He low-temperature thermochronology data from the footwall of several border faults that augments previously collected data from the Paleozoic-Mesozoic Shire Graben (Castaing, 1991), the Cretaceous Chilwa Alkaline Province (Eby et al., 1995), and the northern Malawi Rift (Van der Beek et al., 1998; Mortimer et al., 2016). Using the Malawi Rift as a case study, we contribute to the longstanding question of how strain is accommodated and transferred along rifts over time. The cooling ages of footwall rocks resulting from this study provide an important basis for comparison of the strain accommodation along the Malawi Rift and the Shire Rift.

The understanding of the timing of tectonic processes and associated strain accommodation and strain rates is important for providing insights into how continental rift systems evolve during their early stages and how these processes relate to tectonic activities along plate boundaries. The linking and interaction between adjacent rift segments, as they propagate, typically occurs where structurally complex areas (e.g., transfer zones) have allowed along-axis changes in subsidence of grabens and elevation of uplifted flanks (Rosendahl, 1987; Morley et al., 1990; Faulds and Varga, 1998; Morley, 1999). Analog and experimental models reveal 5 potential types of rift linkage across basins: three types where rifts bend away from the inherited structure (connecting via a wide or narrow rift or by forming a rotating microplate), a type where rifts bend towards it, and straight rift linkage (Brune et al., 2017). Strain is concentrated in these areas of rift linkage to take up displacement variations along the faults and to accommodate space problems created by fault interaction (Bell et al., 2014). Kolawole et al. (2021) also investigated and broadened the classifications of the processes and patterns of linkage in early-stage rift systems along their interaction zones.

Extension accommodated along continental rifts, especially at the early stages, remains vital to the understanding of the dynamics of the processes and products of plate tectonics. Strain accommodation, or the style or pattern of strain in the upper crust during continental rifting is usually manifested by the formation, propagation, and linkage of normal faults and rift basins (Muirhead et al., 2019; Nixon et al., 2016, Calais et al., 2008). Strain accommodation and transfer control the architecture and geometry of early-stage continental rifting, as often observed in the active border faults and other fracture systems along the rift axes (Muirhead et al., 2019; Nixon et al., 2016) which preserve and provide information about the deformation history of the rift. Thorough knowledge of the models of continental rifting at their early stage will help with seismic hazard mitigation as most of the extension along rift basins is accommodated along the border faults and have the potential to host earthquakes (Foster and Jackson, 1998; Craig et al., 2011, Ebinger et al., 2019). Rift basins are also one of the major locations for hydrocarbon accumulation (Macgregor, 2015). Therefore, it is vital to provide accurate geometry of structures and timing of deformational processes in early-stage continental rifting due to their economic and hazard implications.

2 Tectonic Setting and Previous Thermochronology in the Study Area

The Malawi Rift is an approximately 750 km long rift (Ebinger et al., 1989) at the southern end ofin the Western Branch of the ~4,000 km-long East African Rift System (EARS; Fig. 1). The Malawi Rift propagates from the Rungwe volcanic province in the north towards the south and ends against the older Shire Rift (e.g. Specht and Rosendahl, 1989). Specht and Rosendahl (1989) observed through seismic imaging that the 2 to 3 km sedimentary fill thickness of the Malawi Rift in the north of the rift gradually decreases towards the south as the rift reaches the Shire Rift (Figure 1) leading them to propose that rift initiation propagated southward over time.

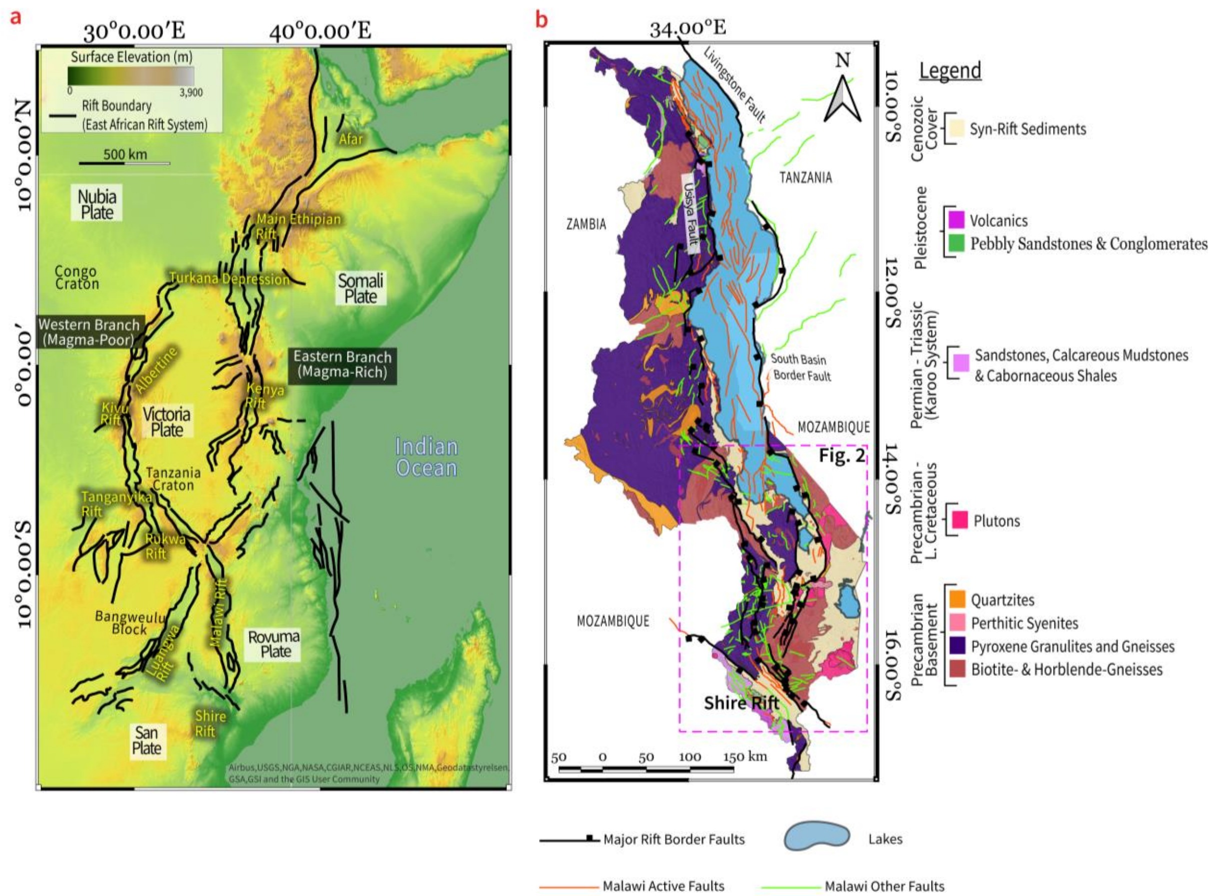

Figure 1: (a) Structural map of the East African Rift Sytems shown on an elevation map. The black lines highlight the major rift bounding faults along each rift system. (b) Geologic and structural map of the Malawi Rift and Shire Rift highlighting the major border faults. (Modified from Bloomfield et al., 1965)

The Malawi Rift can be sub-divided into 8 distinct grabens and half grabens of about 100 –150 km in length with the orientation along strike of the faultsvarying along its axis (Laó-Dávila et al., 2015). The southern Malawi Rift is composed of the Makanjira Graben, Malombe Graben and Zomba Graben. The Bilila-Mtakataka Fault , Malombe Fault , Zomba Fault , Lisungwe Fault are contained in the major grabens (Fig. 2). Other smaller border faults associated with the grabens in the Shire Rift include the Thyolo and Muona Faults, Mwanza Fault, etc. (Figure 2).

One of the fundamental debates about the evolution of the Malawi Rift (and mechanisms and models of continental rift growth in general) is whether strain accommodation started at the same time but at different rates along the Malawi Rift or if strain accommodation started at different times and propagated along the rift. The question of why the Northern Malawi Rift seems to have border faults that are considered to be mechanically incapable of accommodating more strain because they have reached their maximum length and displacement (Muirhead et al., 2016; 2019; Wedmore et al., 2020) whereas the Southern Malawi Rift which has similar border faults in terms of length, is still accommodating strain, has brought about quite a fewproduced different hypotheses over the years. The debate centers on whether there was a chronological southward progression of rift initiation in a zipper-like fashion (Vink, 1982; Specht and Rosendahl, 1989) versus a coeval opening model of continental rifting initiation with a gradual decrease in total extensional strainextension to the south (Saria et al., 2013; Stamps et al., 2008; 2018; 2021). Another plausible explanation is a coeval onset of Malawi Rift initiation along its length, with strain accommodated at faster rates along the rift across the northern part relative to the southern part of the rift with respect to the location of the Euler pole of rotation for the two divergent plates (Nubian and Rovuma plates; Saria et al., 2013; Stamps et al., 2021).

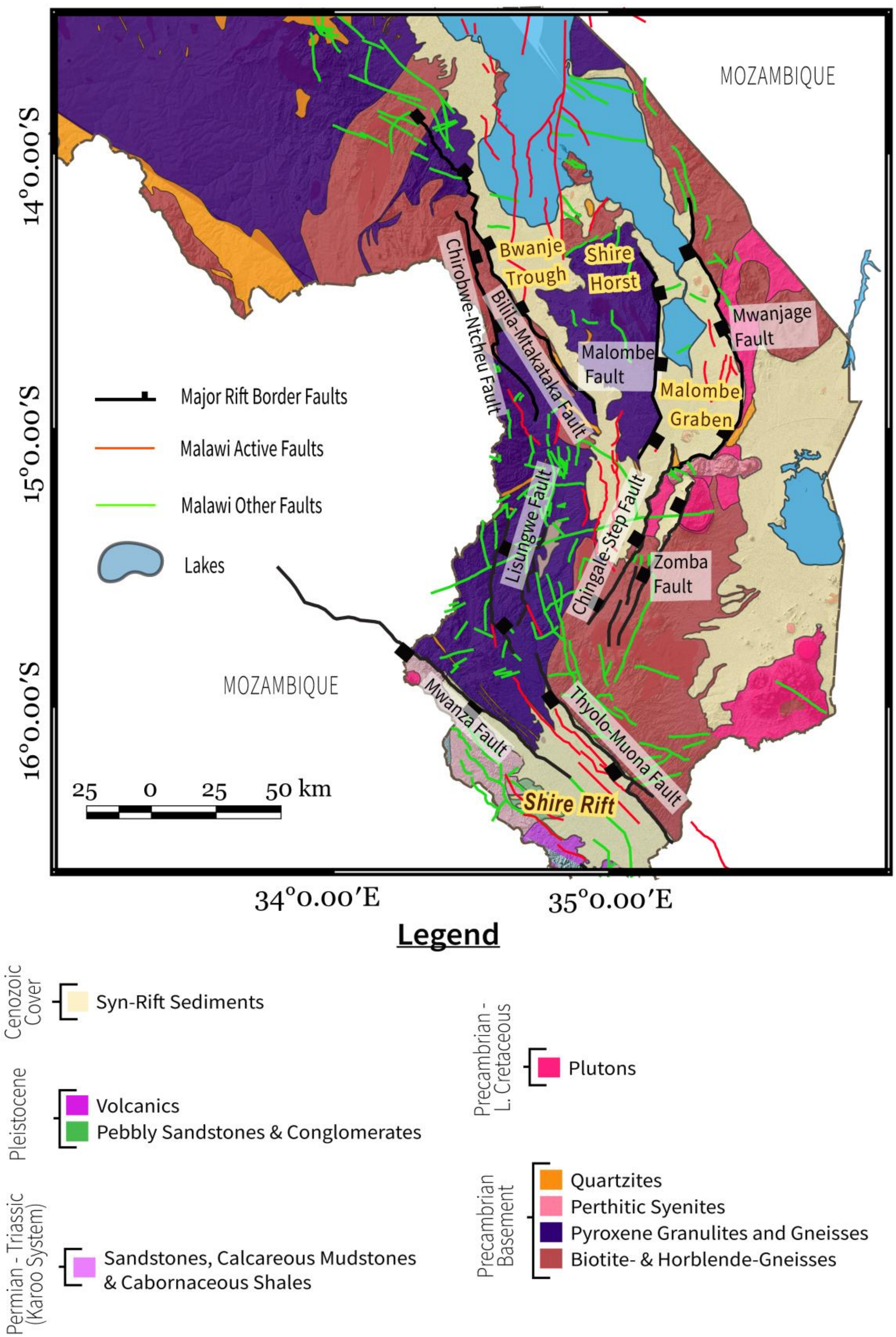
MOZAMBIQUE
14°0.00′S
15°0.00′S
16°0.00′S
34°0.00′E
35°0.00′E
Bwanje Trough
Shire Horst
Chirobwe-Ntcheu Fault
Bilila-Mtakataka Fault
Mwanjage Fault
Malombe Fault
Malombe Graben
Lisungwe Fault
Chingale-Step Fault
Zomba Fault
Mwanza Fault
Thyolo-Muona Fault
Shire Rift
MOZAMBIQUE
Major Rift Border Faults
Malawi Active Faults
Malawi Other Faults
Lakes
25 0 25 50 km
Legend
Cenozoic Cover
Syn-Rift Sediments
Pleistocene
Volcanics
Pebbly Sandstones & Conglomerates
Permian - Triassic (Karoo System)
Sandstones, Calcareous Mudstones & Cabornaceous Shales
Precambrian - L. Cretaceous
Plutons
Precambrian Basement
Quartzites
Perthitic Syenites
Pyroxene Granulites and Gneisses
Biotite- & Horblende-Gneisses

Figure 2: Geologic map of the study area, which includes the southern Malawi Rift and Shire Rift, showing the different geologic units and the major fault systems. The black text highlighted in yellow gives information about the rift, grabens, horst or trough that host the different fault networks along/across the rift.

The ages of tectonic deformation in the region have been established through the recognition of correlations between the deformation, emplacement of magmatic bodies, and sedimentation. For example, Castaing, (1991) identified three major episodes of tectonic activity: the Karoo rifting period (Late Carboniferous to Early Jurassic), the post-Karroo alkaline igneous activity (Middle Jurassic to Cretaceous), and the East African rifting (Cenozoic to Recent). Orientations of each of the tectonic events were established from structural analysis of the fracture systems (Castaing, 1991).

The tectonic and denudation history, uplift and isostatic rebound of the footwall blocks, and deformation associated with igneous intrusions of certain parts of the Malawi Rift have been previously investigated using low temperature apatite fission-track (AFT) and (U-Th)/He (AHe) analysis (Eby et al., 1995; Van Der Beek et al., 1998; Dazinnes et al., 2011; Mortimer et al., 2016). Van Der Beek et al. (1998) used inverse thermal modeling of AFT data to reconstruct a thermal history that suggests distinct repeated phases of uplift and denudation of the rift flanks along the Livingstone Fault in the northern part of the Malawi Rift at 250–200 Ma, 150 Ma, and 140–50 Ma. Mortimer et al., (2016) adopted AHe dating to investigate the along-strike and vertical distribution of cooling ages along the Livingstone fault, which is the bounding fault system of the Karonga Basin of the northern Malawi Rift. They used age-elevation relationships to show that regional-scale cooling associated with Cenozoic rifting of the northern Malawi Rift began at ∼23 Ma and that AHe thermochronology can record segmentation and linkage of border faults. Eby et al. (1995) and Dazinnes et al. (2011) used AFT analysis to estimate the age of the igneous intrusions in the Chilwa Province of southern Malawi adjacent to the main rift. Even though these studies have provided insight into of the tectonics of the Malawi Rift, there remains a knowledge gap in the thermochronological and tectonic history of early-stage rifting along the border faults of the Southern Malawi Rift and older Shire Rift to the south that we address in this study.

3 Methods

We applied low-temperature AFT and AHe thermochronology and remote sensing to understand the interaction between timing and tectonic uplift during the evolution of the southern part of the Malawi Rift and the northern Shire Rift. AFT and AHe dating were used to determine the thermal history of the footwall blocks of several major border faults along both rifts to estimate the time of onset of faulting, fault throw, fault displacement, and extension. Apatite fission tracks anneal at low temperatures between 130–60° C over geologic timescales (Reiners and Brandon, 2006) and thus record the thermal history of samples subject to tectonic exhumation processes of brittle deformation taking place in the upper continental crust (~2–5 km). Even though AHe and AFT results are presented as dates (referred to as cooling ages in this study), they typically do not indicate cooling through the closure temperature nor the date of a particular geologic event. The dates instead capture the integrated thermal history of the apatite since the onset of helium retention and/or radiation damage accumulation. This is the reason why inversion models (e.g., Ketcham, 2005) are at the core of making thermochronologic measurements and geologic interpretations to constrain this thermal history. The geometry of structures along the Southern Malawi Rift and Shire Rift was also investigated by remote sensing analysis of satellite digital elevation model data (SRTM-DEM) through the application of hillshade imaging, as well as slope analysis coupled with the available data from the Malawi active fault database (Williams et al., 2021; Kolawole et al., 2021).)

3.1 Apatite Fission Track Measurement

The application of AFT thermochronology is well-established in extensional tectonic settings where cooling is a product of both tectonic footwall exhumation, and erosional exhumation of uplifted footwall blocks (Fitzgerald et al., 1991; Foster et al., 1991; Ehlers et al., 2001; Stockli, 2005). Here we have applied AFT dating to investigate the timing and magnitude of upper crustal (2-5 km; 60–130 °C) cooling and exhumation ages associated with footwall uplift on 13 rock samples (gneisses, syenite, foliated granite, and granite dikes) collected from the footwall blocks of several extensional border faults (Fig. 2). Mineral separation was undertaken at Zirchron LLC, Geoscience Services using electro pulse disaggregation. The fission-track mounting, calibration, and measurement were done at the University of Arizona

Fission Track Laboratory. Apatite sample irradiation was carried out at the Oregon State University Radiation Center.

The AFT ages were measured by using the External Detector Method (EDM) with ages calculated using the zeta calibration of Hurford and Green (1983) using independent age standards including Durango and Fish Canyon Tuff apatite. This method involves counting the spontaneous track density in a selected grain and finding the exact mirror image of the counted area on the corresponding muscovite/mica external detector where the induced track density is counted over the same area. A geometry factor of 0.5 was used to correct for the difference in the geometry of track registration for the internal surface on which the spontaneous tracks are measured and the external detector surface used for induced tracks (e.g. Wagner and van den Haute, 1992). Apatite crystal grains were carefully selected, with only grains with the highest etching efficiency (parallel to the c-axis) selected for counting and horizontal confined track length measurement (e.g. Gleadow, 1978).

3.2 Apatite (U-Th)/He (AHe) Measurement

For rocks undergoing steady cooling, the AHe ages record the time since these samples were closed for He diffusion at temperatures below ~70 °C (at geologic cooling rate of 10 °C/Ma, Reiners & Brandon, 2006). Thus, this technique is particularly sensitive to tectonic processes active in the uppermost part of the crust. The AHe dating technique is based on the production of alpha particles (^{4}He) as a result of radioactive decay of isotopes of the elements U, Th, and Sm (Farley et al., 1996). The concentrations of the parent isotopes and ^{4}He can thus be used to calculate the AHe cooling age. For apatite, the measurements were done using a two-stage analytical procedure involving degassing of the crystal by heating and gas source mass spectrometry to measure ^{4}He, followed by inductively-coupled plasma mass spectrometry on the same crystal to measure U, Th and Sm.). Helium diffuses through a crystal at a certain rate which is dependent on the time, temperature, grain size, and radiation damage. He starts to be retained within apatite crystals at ~80 °C, and becomes fully retained at ~30 °C (a range of temperatures known as the AHe partial retention zone or PRZ). As part of this study, we undertook exploratory AHe analysis on two samples: one from the footwall of the Malombe Fault of the southern Malawi Rift (LM 8B) and one from the footwall block of the Thyolo Fault on the northern margin of the Shire Rift (SE 5-1). We analyzed 10 apatite grains, 5 grains from each sample. The apatite grains were handpicked based on the quality of the grain and their suitability for AHe age analysis. The AHe age analysis was carried out at the University of Arizona Radiogenic Helium Dating Laboratory.

3.3 Inverse thermal history modeling

AlthoughJust as we have mentioned earlier that although AHe and AFT results are presented as dates (referred to as cooling ages in this study), they typically do not indicate cooling through the closure temperature nor the date of a particular geologic event. The dates instead capture the integrated thermal history of the apatite since the onset of helium retention and/or radiation damage accumulation. Hence, the need to conduct thermal history modeling. A given fission-track length distribution can be related quantitatively to thermal history, using a mathematical description of the annealing process (e.g. Ketcham et al., 2007). Therefore, the lengths and angle to c-axis of horizontal confined fission tracks were measured in each of the samples to help constrain the thermal history that most likely predicts the measured data using inverse thermal modeling software HeFTy version 1.9.3 (Ketcham, 2005) using the AFT annealing model of Ketcham et al. (2007) without modeling c-axis projected lengths, and Dpar (etch-pit diameter parallel to the c-axis) as an additional kinetic parameter. The inversion models yield time-temperature paths consistent with geologic constraints and thermochronometric observations by taking kinetic models that describe how the AHe and AFT systems respond as a function of temperature and time. Laboratory experiments show that the thermal annealing of fission tracks in apatite obeys a so-called fanning curvilinear relationship, in which the degree of shortening depends on both the amount and duration of heating. The HeFTy program uses a Monte Carlo method that generates AFT data from large numbers of thermal histories according to the Ketcham et al. (2007) AFT annealing model and uses the p-value of formalized hypothesis tests (in this case the chi-square test) to assess the goodness of fit of the model predicted data with the measured data, and thus decide which t–T paths to retain or reject. We used 20 ± 5°C as present-day temperature, two constraint boxes, default values for other parameters for inverse modeling of all the samples. The first main constraint box covers 200-5 Ma and 20-180°C to account for tectonic events which include the Gondwana breakup and the subsequent Karoo rifting, alkaline igneous intrusions, and the more recent East African rifting, which span this geologic time (Castaing, 1991; Eby et al., 1995). We used 30-0.1 Ma and 20-100°C for the second constraint box to help provide more details and constraint points on more recent cooling history (Castaing, 1991; Van Der Beek et al., 1998; Mortimer et al., 2016). The second constraint box provides more details on the thermotectonic history of the East African rifting along the Malawi Rift which has been constrained and suggested to have initiated around this time in the region. HeFTy was run until 100 time-temperature paths were found that predicted a good fit with the measured data. For sample SW7-1 no good fit paths could be found, thus this was run until 100 acceptable paths were found.

We also ran HeFTy to include our new AHe data for samples LM8B and SE5-1 using the AHe Radiation Damage Accumulation and Annealing Model (RDAAM) of Flowers et al. (2009) and AHe alpha stopping distance correction of Ketcham et al. (2011). However, owing to the use of pass or reject formalized statistical hypothesis tests by HeFTy, it tends to fail when trying to predict large data sets that include more precise data (e.g. multiple AHe grain ages from the samples) (Vermeesch and Tian, 2014). As a result, acceptable and/or good fit paths were only obtained only when using the youngest two or fewer AHe grain ages from each sample (see Supplemental Figure S2). Therefore, we also conducted inverse thermal modeling including the AHe data on these two samples with the QTQt modeling software (version 5.8.0, Gallagher, 2012) using measured U, Th, and Sm concentrations, grain size, and He concentrations for the AHe data, in addition to the AFT age, length, and Dpar data. While QTQt uses the same AFT annealing and AHe diffusion models as HeFTy to forward model data, QTQt uses a Bayesian 'Markov Chain Monte Carlo' (MCMC) algorithm for inverse modeling to constrain thermal histories that most likely predict the data. This offers the advantage of always producing a best-fitting thermal history, even for large and precise data-sets, The disadvantage of QTQt is that the most-likely thermal history may not adequately predict the input data, making it essential to check the observed versus predicted results to allow an informed, but nevertheless subjective comparison of how well the data predicted by most likely thermal history match the measured data (Vermeesch and Tian, 2014). For the QTQt inverse modeling we set a broad time-temperature space (ranges for general prior) for thermal history sampling of 100±100 Ma and 110±90 °C, and a present-day temperature of 20±5 °C, allowed no reheating, with other limits set at default values. For the MCMC sampling, we ran 100,000 iterations (50,000 burn-in and 50,000 post burn-in), a thinning value of 1, and default values for all other options.

3.4 Remote Sensing Analysis

Analysis was carried out on a 30-m resolution Shuttle Radar Topography Mission (SRTM) digital elevation model (DEM) using QGIS and ENVI software to map major lineaments systems of the study area. A hillshade map was created from the SRTM-DEM using the sun angle of 45^{o} and azimuth of 315^{o} to highlight the major faults in the study area. Geologic structures can be easily mapped from the hillshade map superimposed with a pseudocolored DEM to illustrate the variations in elevation across the rift system. We measured and interpreted the orientation of regional faults and minimum scarp heights of major border faults which are essential parameters in delineating tectonic conditions from the mapped faults.

A slope map was also created from SRTM-DEM using QGIS. Slope analysis was done to also delineate the geologic structure along the accommodation zone between the Southern Malawi Rift and Shire Rift. The pattern of change in slope or dip of geologic structures provides information on the tectonic setting and architecture of the structures at the surface. Structures like relay ramps, which are usually found across accommodation zones, are indicative of linkage and transfer of strain between geologic structures. Breached relay ramps have a certain dip or slope angle (10 – 15° for recently breached relay ramps), which was used to characterize this region for structures that could facilitate strain transfer (Fossen and Rotevatn, 2016 and references therein). All faults mapped were verified and also augmented by previously mapped faults in the region (see Williams et al., 2021 and Kolawole et al., 2021 for details)

SRTM-DEM hillshade and slope maps were used to map faults along the rift border faults. The mapped faults from the hillshade and slope maps combined with faults mapped from Kolawole et al. (2021) and Williams et al. (2021) were used to generate a density plot of the fault systems. The density plot of the faults can help determine the model of rift linkage (Brune et al., 2017) and the potential for strain transfer can be interpreted and inferred from the geometry.

3.5 Estimation of Strain Rates along Southern Malawi Rift vs Northern Malawi Rift

Exhumation is the vertical motion of rock towards the Earth's surface (England and Molnar, 1990). We estimated the extension and displacement which are forms of strain and the respective strain rates (extension rates and slip rates) from the uplift or exhumation calculated from our AFT modeling of the samples as done in Foster (2019). To estimate the extension and displacement along a fault requires knowledge of the heave or dip of the fault. Effective constraints on the timing of the uplift, which can be estimated from AFT measurements and modeling, make it possible to determine the strain rates. Time constraints on exhumation were directly established by the cooling ages that are set during cooling across the closure temperature isothermal surface (Tc).

To calculate an average exhumation rate from a single sample, the paleo-geothermal gradient i.e., the vertical distance between the Tc and Earth's surface during exhumation, has to be independently known (e.g., Wagner et al. 1977). Generally, a geothermal gradient of 25 – 30 °C/km is assumed for most tectonic settings across the surface of the Earth. Such values have been confirmed by Van Der Beek et al. (1998) from heat flow in the Earth's crust across the northern Malawi Rift. The estimation of Curie depth and temperature from aeromagnetic data by Njinju et al. (2019) across the Malawi Rift gives a more precise variation of the geothermal gradients along the faults and was adopted in this study. Thus, cooling rates in this study were converted to exhumation rates assuming a geothermal gradient of 25 °C/km. We assumed isostasy is responsible for the uplift of the footwall in response to the extension occurring across the rift. The exhumation was calculated for each sample as the difference between the highest temperature at the initiation of the most recent thermal episode (acceptable fit) and the present-day temperature (20^{o} C) divided by the geothermal gradient. For this study, the estimated amount of exhumation was assumed to be the maximum amount of vertical uplift along the faults and used in the estimation of the strain rates along the fault.

The strain accommodated in the southern Malawi Rift was calculated using the relationships shown in equations 1 and 2 below;

$$\text{Displacement } = \frac{\text{Uplift}}{\sin\alpha};$$

$$Heave = \frac{Uplift}{\tan\alpha} \qquad \text{Eqn. 1}$$

Where α is the dip of the fault (assumed to be 45°, 60°, or 75° for the Malawi Rift) (Muirhead et al., 2016; Stevens et al., 2021; Ojo et al., 2022). Using Eqn. 1 above and timing constrained from AFT modeling, the strain rates for the southern Malawi Rift are calculated as;

$$\text{Strain Rate } = \frac{\text{Strain}}{\text{Time}} \qquad \text{Eqn. 2}$$

4 Data and Results

4.1 Apatite Fission-Track Results

We summarize the thermochronologic data from the Southern Malawi Rift and Shire Rift and integrate it with geologic constraints to determine the evolution of these two rift systems in terms of strain accommodation in the upper crust (2-5 km depth) that spans about 135 Ma. AFT central ages range between 128 ± 6 Ma and 60 ± 4 Ma, while mean track lengths (MTLs) range between 13.35 μm and 11.02 μm (Tables 2 and 3). AFT ages show no obvious trend versus elevation, although this is to be expected given the large geographic spread and the small elevation difference between samples. Our results are consistent with Eby et al. (1995) and Daszinnies et al. (2008; 2009) who measured AFT ages of the alkaline igneous intrusions near the rift shoulders of the southern Malawi Rift. The range of cooling ages from these studies matches well with this study which is focused on the footwalls of several of the main rift border fault scarps to obtain information on the nature and timing of faulting (Fig. 3).

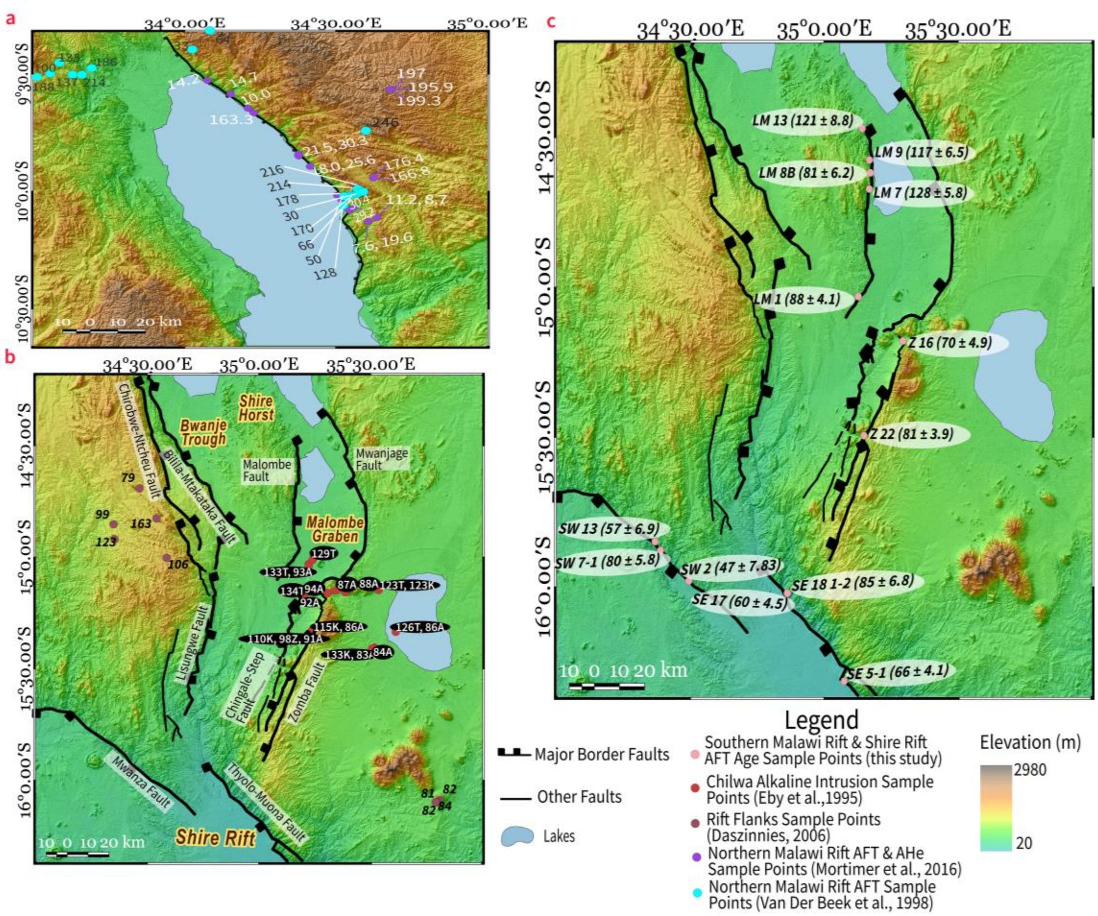

Figure 3: (a) Hillshade Map of the northern Malawi Rift showing the low-temperature thermochronogy results of rock samples along the Livingstone Fault. Teal circles and black text are rock sample locations and AFT results from Van Der Beek et al. (1998) while purple circle and white text are locations of rock samples and AHe results from Mortimer et al. (2016) (b) Map of southern Malawi Rift showing the major border faults highlighted and the location of the samples from Eby et al (1995) with corresponding AFT (A), K/Ar (K), and Titanite (T) ages in millions of years and samples from Daszinnies 2006. The brown intra-rift faults highlighted in brown are from Wedmore et al., (2020). (c) Map of southern Malawi Rift showing the major border faults highlighted and the location of the samples collected for this study. It shows the sample ID and their corresponding AFT ages.

Table 1: AFT Sample Location and Elevation data

Samples	***Latitude***	***Longitude***	***Elevation (m)***
Malombe Fault			
LM 9	-14.5740	35.1678	598
LM 1	-15.0297	35.1266	539
LM 7	-14.6709	35.1676	579
LM 8B	-14.6169	35.17185	576
LM 13	-14.4687	35.1418	579
Chingale-Step Fault			
Z 16	-15.1779	35.2932	803
Z 22	-15.4938	35.1476	773
Thyolo Fault			
SE 5-1	-16.3134	35.0738	201
SE 18 1-2	-16.0193	34.8635	335
SE 17	-16.0198	34.8608	305
Mwanza Fault			
SW 7-1	-15.8764	34.3879	306
SW 2	-15.9788	34.4935	247
SW 13	-15.8475	34.3672	495

Table 2: Fission-track Data

Sample	***No. of Crystals***	***Track Density (x 10^6 tracks.cm^{-2})***			***Age Dispersion***	***Central Age(Ma)***	***Apatite Mean Track Length***	***Standard Deviation***
		ρs (Ns)	***ρi (Ni)***	***ρd (Nd)***	***(Pχ2)***	***(±1σ)***	***(μm ± 1 s.e.) (no. of tracks)***	***(μm)***
LM 1	20	2.295 (2446)	6.458 (6882)	1.608 (5145)	10.6% (0.16%)	**87.4±4.1**	**13.01±0.16 (99)**	**1.55**
LM 7	20	2.341 (1516)	4.532 (2935)	1.594 (5101)	3.5% (47.3%)	**124.8±5.6**	**12.43±0.16 (101)**	**1.60**
LM 8B	20	2.902 (302)	0.8543 (889)	1.580 (5057)	1.4% (64.9%)	**81.6±6.0**	**12.94±0.12 (100)**	**1.21**

LM 9	20	1.138 (1413)	2.318 (2878)	1.566 (5013)	12.8% (0.99%)	**117.2±6.3**	**12.15±0.16 (100)**	**1.63**
LM 13	20	1.519 (1750)	2.844 (3276)	1.553 (4969)	23.3% (<0.01%)	**122.6±8.4**	**11.94±0.18 (101)**	**1.84**
SE 5-1	20	0.602 (482)	2.130 (1705)	1.539 (4925)	(5.93%) (64.24%)	**66.1±4.1**	**11.02 ± 0.18 (98)**	**1.82**
SE 17	20	0.3540 (389)	1.381 (1518)	1.525 (4480)	13.2% (17.2%)	**59.9±4.3**	**12.33±0.15 (100)**	**1.51**
SE 18-1-2	20	0.4424 (310)	1.214 (851)	1.511 (4836)	0.03% (88.3%)	**83.6±6.1**	**13.18±0.14 (104)**	**1.44**
SW 2	20	0.09723 (85)	0.2883 (252)	1.382 (4422)	<0.01% (99.8%)	**79.5±10.2**	**-**	**-**
SW 7-1	20	0.5927 (374)	1.670 (1054)	1.484 (4748)	8.3% (36.1%)	**80.1±5.7**	**12.74±0.10 (100)**	**1.02**
SW 13	20	0.2474 (146)	0.9389 (554)	1.470 (4704)	26.1% (10.7%)	**58.5±6.8**	**12.83±0.18 (81)**	**1.63**
Z 16	20	0.3465 (361)	1.080 (1125)	1.456 (4660)	<0.01% (99.8%)	**71.0±4.8**	**13.35±0.12 (100)**	**1.19**
Z 22	20	2.283 (1081)	6.193 (2933)	1.442 (4616)	0.75% (58.2%)	**80.8±3.8**	**12.49±0.15 (107)**	**1.51**

Notes:

(i). Analyses by external detector method using 0.5 for the $4\pi/2\pi$ geometry correction factor;

(ii). Ages calculated using dosimeter glass: IRMM540R with ζ_{540R} = 305.8±8.4 (apatite);

(iii). $P\chi^2$ is the probability of obtaining a χ^2 value for v degrees of freedom where v = no. of crystals - 1;

(iv). s.e. = Standard Error.

The relationship between the fission-track ages and the mean confined track lengths for each sample is shown in a boomerang plot (Green, 1986; Gleadow et al., 1986) in Figure 4. Except for sample SE 5-1, the data show short mean track lengths (< ca. 13 μm) and a general trend of increasing mean lengths with decreasing age. Such a pattern allows a qualitative assessment of the thermal history of these samples (e.g. Gallagher and Brown, 1997) indicating a cooling episode in the last ca. 50 million years (younger than the youngest AFT age) from temperatures within the AFT partial annealing zone (ca. 60-120 °C).

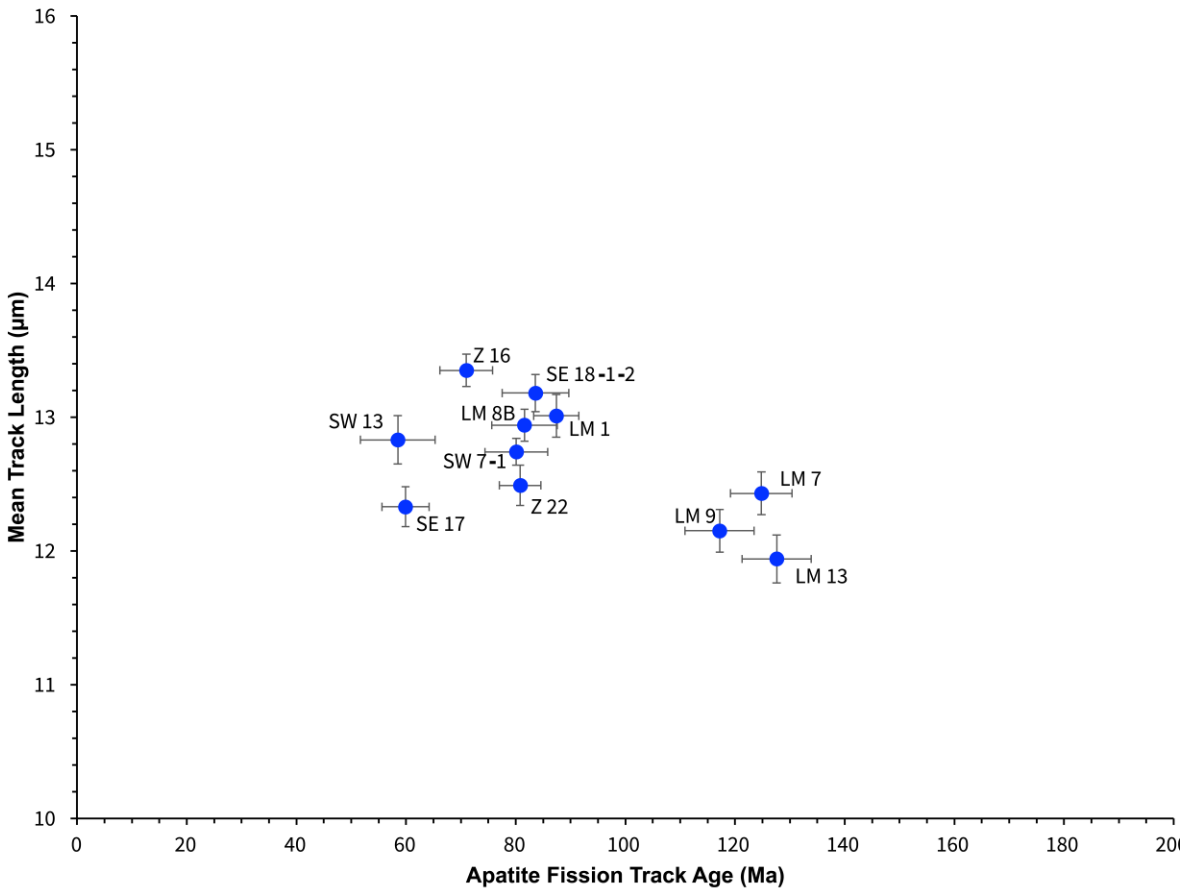

Figure 4: Plot showing the relationships between the sample AFT ages (Ma) vs the measured confined mean track lengths for each of the 12 samples used in this study for the thermal history modeling. One sample (SW2) was omitted because of the lack of confined fission tracks in the sample.

4.2 Apatite (U-Th)/He Dating Results

The corrected AHe ages (Table 3; see Supplemental Table T1 for the more complete data) range from 52.4 ± 0.7 Ma to 14.3 ± 0.2 Ma for the two rock samples (LM 8B and SE 5-1) with the age distribution consistent with the distribution of sampling for AFT cooling ages. Cenozoic ages occur for all 10 apatite grains analyzed from the 2 rock samples. Sample LM 8B along the Malombe Fault (LM8B_Ap1-5) in the Southern Malawi Rift has corrected AHe ages that range from 41.8 ± 0.7 to 30.2 ± 0.7 Ma and also shows a positive trend of age with eU (effective uranium concentration). This is a combined measure of U, Th, and Sm decays ([eU] =

[U] + 0.235[Th] + 0.0046[Sm]), and thus provides an estimate of radiation damage. Sample SE 5-1 along the Thyolo Fault (SE 5-1_Ap1-5) in the Shire Rift has corrected AHe ages that range from 52.4 ± 0.7 to 14.3 ± 0.2 Ma. Data from SE 5-1 are a little more complex and show no obvious age vs eU trend (see Supplemental Figure S1).

Table 3: Apatite-Helium Data

Sample Analysis	raw date (Ma)	1s ± date (Ma)	corr date (Ma)	1s ± date (Ma)	ppm eU w/ Sm (Ca)
LM8B_Ap1	29.5	0.6	41.8	0.7	19.0
LM8B_Ap2	28.8	0.4	38.5	0.6	9.4
LM8B_Ap3	27.2	0.4	34.1	0.4	6.7
LM8B_Ap4	20.8	0.5	30.2	0.7	8.3
LM8B_Ap5	28.2	0.4	38.1	0.5	10.2
SE5-1_Ap1	25.7	0.4	37.2	0.5	18.2
SE5-1_Ap2	34.2	0.4	52.4	0.7	17.6
SE5-1_Ap3	13.0	0.2	17.3	0.2	27.0
SE5-1_Ap4	18.6	0.3	26.4	0.4	26.3
SE5-1_Ap5	10.0	0.1	14.3	0.2	12.1

4.3 Outcomes of Inverse Thermal Modeling of the Thermochronological Data

Inverse modeling (e.g., Ketcham, 2005) was used to constrain the thermal histories of our 13 rock samples across the Southern Malawi Rift and the Shire Rift, and forms the basis of geologic interpretations from thermochronologic measurements. Results from the modeling of the AFT data only are shown for the southern Malawi Rift in Figures 5 and 6, and the Shire Rift in Figures 7 and 8. and are summarized below. Inclusion of AHe data into inverse modeling from sample LM8B from the Malombe Fault of the southern Malawi Rift, and sample SE5-1 from the Thyolo Fault on the northern margin of the Shire Rift), is dealt with separately in section 4.4 below.

4.3.1 The southern Malawi Rift

We conducted thermal modeling on seven samples from two main rift border faults (Figure 3b), 5 samples from along the Malombe Fault (labeled LM in Fig. 3c), and two samples from along Chingale-step Fault (Labeled Z in Fig. 3b). The best-fit thermal histories from all samples exhibit three periods of cooling.

The results from thermal modeling of the AFT data from the 5 samples along the Malombe Fault are shown in Figure 5. Modeling results from three of the samples show an initial period of enhanced cooling from temperatures > ca. 120°C (above the closure temperature of fission tracks in apatite) to ca. 60-80 °C between ca. 180 and 140 Ma, whereas two other samples show initial cooling to similar temperatures between ca.100 and 80 Ma. All samples then show slow cooling until about 30-20 Ma (<0.1 °C/Ma), with the onset of a period of rapid cooling from temperatures of ca. 50-60 °C to the surface sometime in the last ca. 25 Ma (Fig. 5).

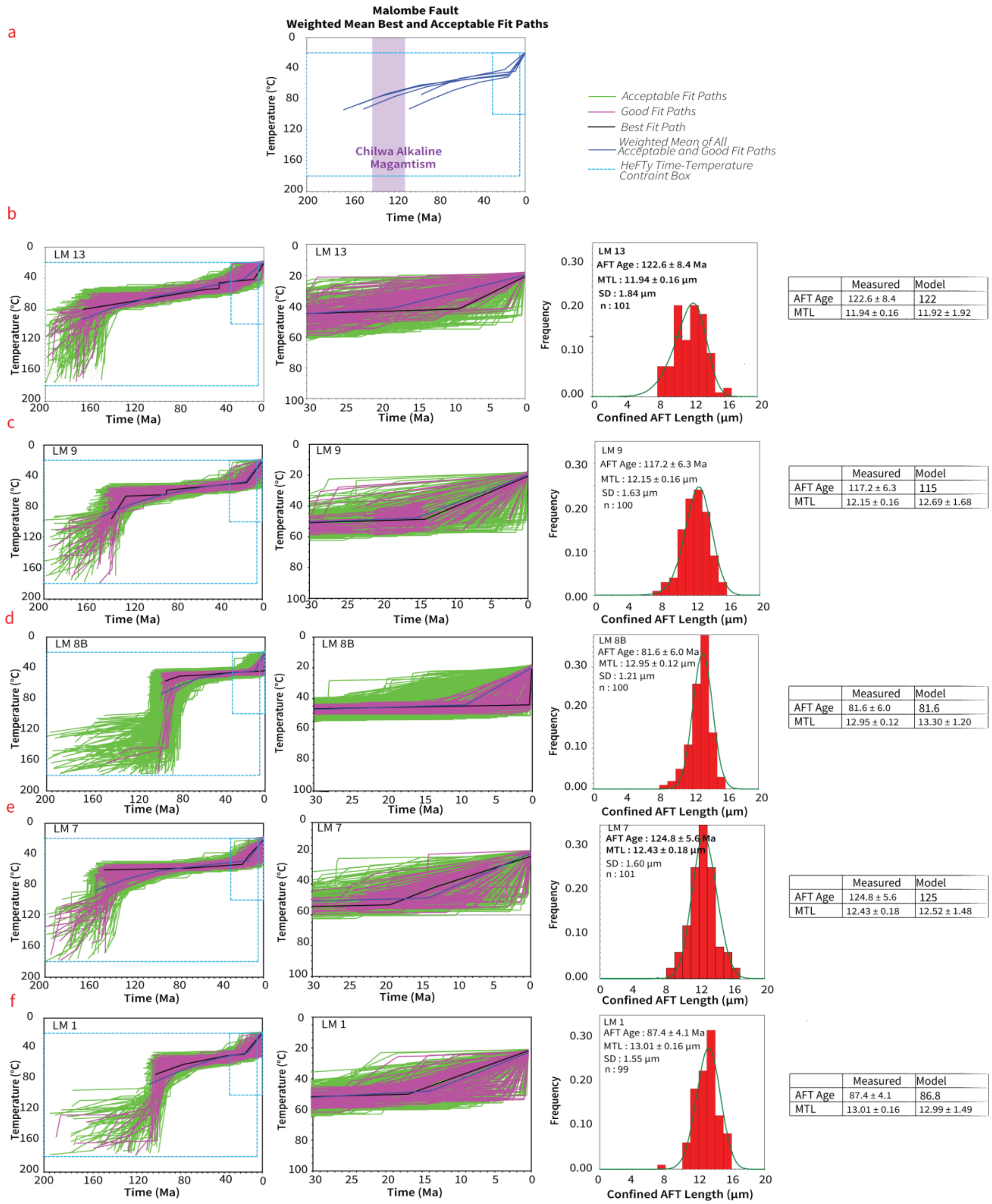

Figure 5: Thermal history models from the southern portion of the Malawi Rift (Makanjira Graben and Malombe Fault) with age and track length distribution prediction outlined. The green paths show time-temperature paths with an acceptable fit, and the pink paths a good fit to the

measured data. The black line is the time-temperature path with the best fit with the measured data (the model data shown in the right panels are predicted from this path), and the weighted mean of all acceptable and good fit paths is shown with the blue line. The figures for each sample are arranged from north to south. (a) showing the weighted mean of all acceptable and good fit paths for all the samples along the Malombe Fault (b) LM 13, (c) LM 9, (d) LM 8B, (e) LM 7, and (f) LM 1.

The two samples from the footwall of the Chingale-step Fault and Zomba Fault both show an initial rapid cooling period from temperatures > ca. 120 °C to ca. 40-80°C between 90 and 75 Ma), followed by slow cooling from 70 Ma until ca. 15 to 5 Ma, followed by a final period of rapid cooling from temperatures of 40-50 °C to the surface since about 15 to 5 Ma (Fig. 6).

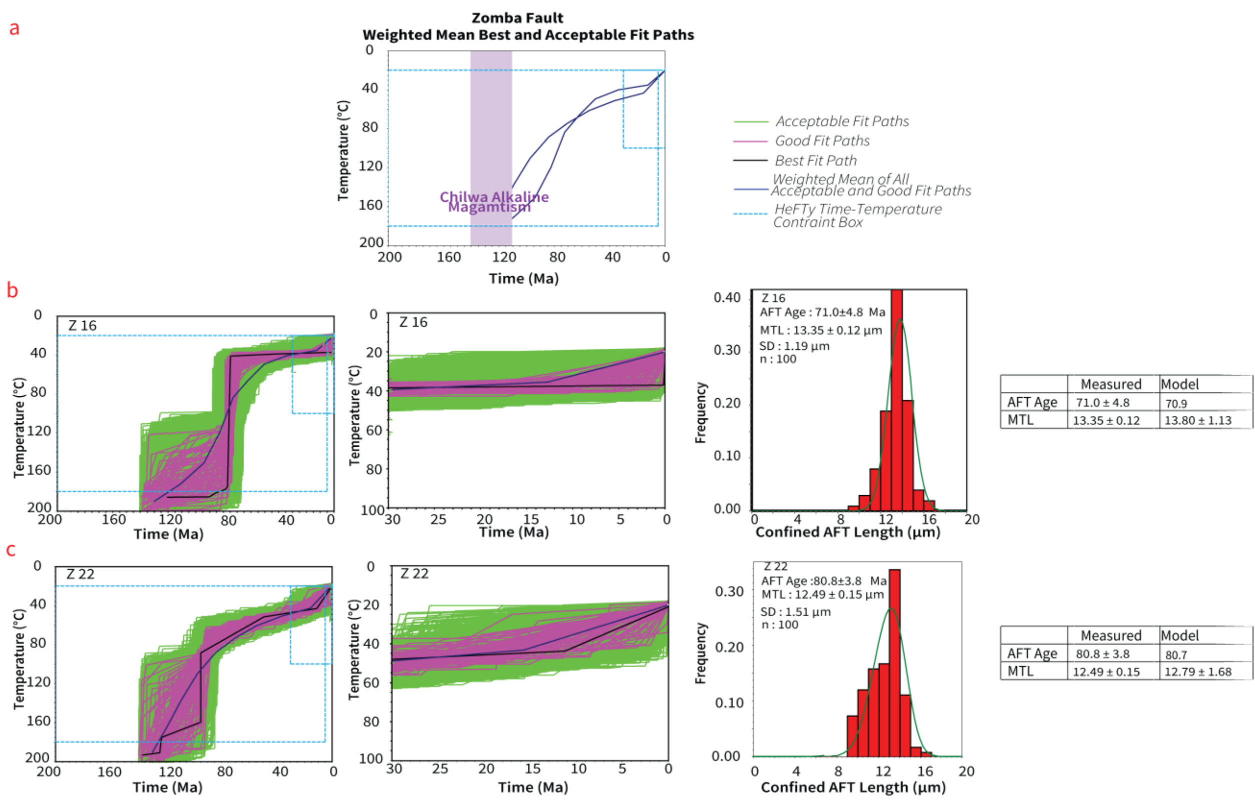

Figure 6: Thermal history models from the southern portion of the Malawi Rift (Zomba Graben, Chingale-step Fault, and Zomba Fault) with age and track length distribution prediction

outlined (a) showing the weighted mean of all acceptable and good fit paths for all the samples along the Zomba Fault (b) Z16, and (c) Z22 (see Figure 5 caption for the explanation of colors).

4.3.2 The Shire Rift

Modeling was conducted on the AFT data from 5 from 6 samples from two major border faults on the northern margin of the Shire Rift (no horizontal confined track lengths were measurable in sample SW2 owing to its very low uranium concentrations and thus low track density). Three samples were modeled from the footwall scarp of the Thyolo fault, and two samples from the footwall of the Mwanza fault. Similar to the results from the southern Malawi Rift, thermal histories that best predict the data from the Shire Rift border faults show 3 distinct episodes of cooling (Figs. 7 and 8).

The three samples from the Thyolo Fault (Fig. 7) show an initial rapid cooling period from temperatures > ca. 120°C to 40-70 °C between 90 and 65 Ma followed by slow cooling from 60 Ma to 20 Ma, and a period of rapid cooling from temperatures of ca. 40-70°C to the surface sometime in the last ca. 20 Ma.

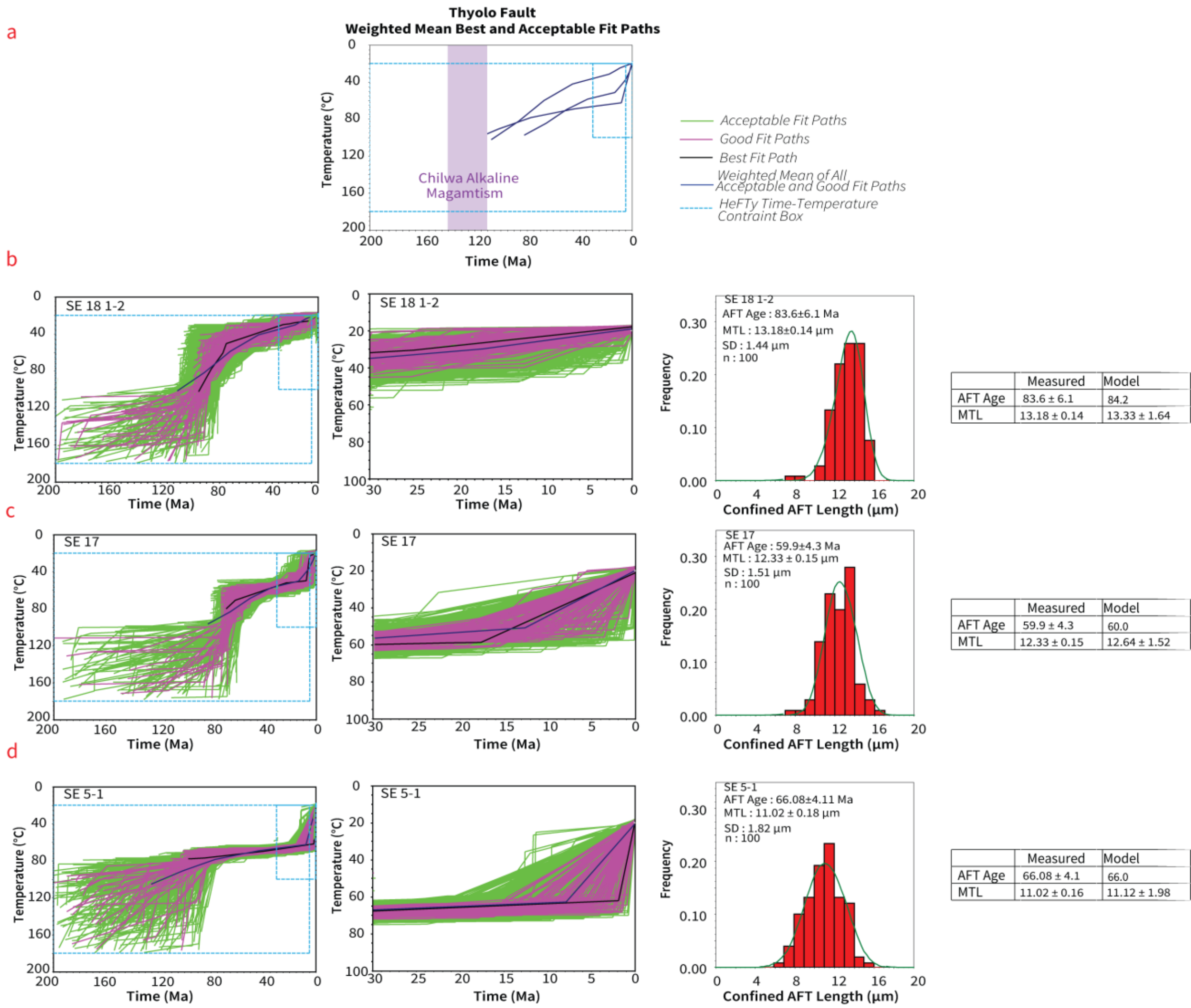

Figure 7: Thermal history models from the northern portion of the Shire Rift (Thyolo Fault) with age and track length distribution prediction outlined (a) showing the weighted mean of all acceptable and good fit paths for all the samples along the Thyolo Fault (b) sample SW7 (c), sample SW13, and (d) sample SE 5-1 (see Figure 5 caption for the explanation of colors).

Modeling results from the two samples along the Mwanza Fault are less well-constrained with only acceptable fit paths found that predicted the measured data for sample SW7-1.. However including both good and acceptable fit paths, then modeling results for both samples along the Mwanza Fault show an initial relatively rapid cooling period between 100 and 70 Ma, followed by slow cooling from 70 Ma to 5 Ma, and, for sample SW7-1 at least, a final period of rapid cooling from temperatures of ca. 50 °C to the surface in the last ca. 10 Ma (Fig. 8).

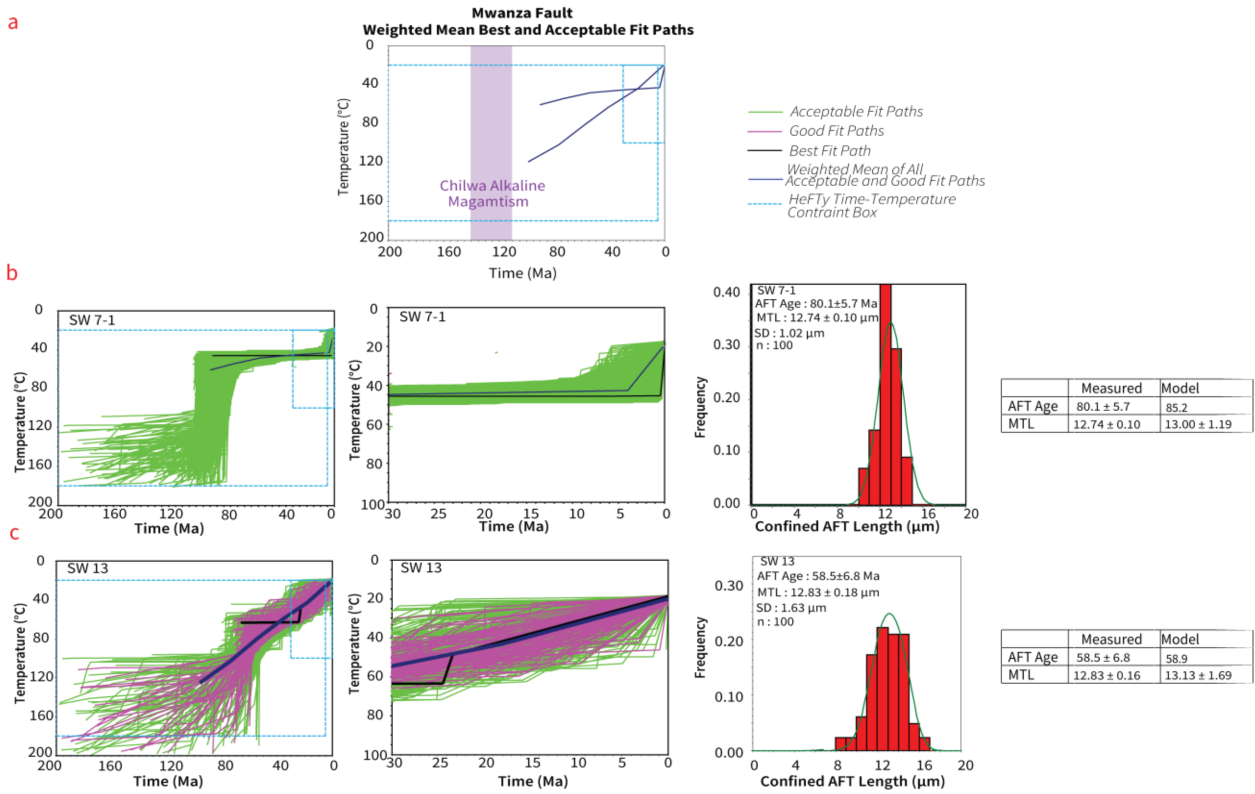

Figure 8: Thermal history models from the northern portion of the Shire Rift (Mwanza Fault) with age and track length distribution prediction outlined. (a) showing the weighted mean of all acceptable and good fit paths for all the samples along the Mwanza Fault, (b) sample SW7, and (c) sample SW13 (see Figure 5 caption for the explanation of colors).

4.4 **Incorporation of Apatite** (U-Th)/He **Data with Apatite Fission Track Data**

The thermal histories of samples LM8B and SE5 1-2 and LM8B from the Southern Malawi Rift and the Shire Rift are presented in Figure 9a and 9b , respectively, were constrained by QTQt inverse thermal history modeling that includes the new AHe data alongside the AFT cooling ages. The modeling results are shown in **Figure** 9 below.

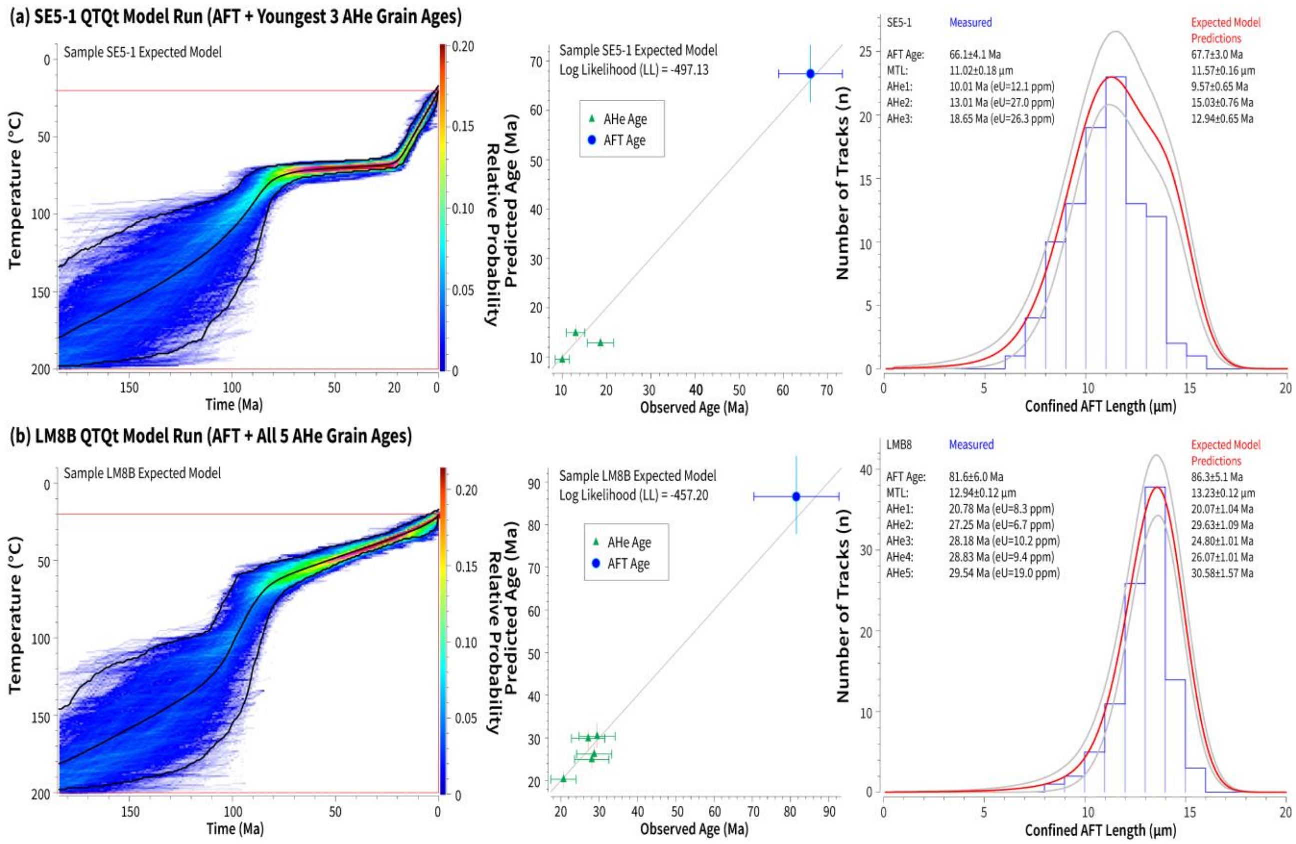

Figure 9: QTQt inverse thermal history modeling results incorporating both AFT and AHe data for samples SE5-1 (a) and LM8B (b). The colored plots on the left show the probability density of the most-likely model thermal histories produced by QTQt, with the black lines showing the preferred Expected Model thermal history with 95% credible intervals (Gallagher, 2012). The central plots show the observed versus predicted age data for the Expected Model, and the plot on the right shows the observed (blue) and predicted AFT length data (red curve with 95% credible intervals in grey). Values for the Expected Model predictions versus observed age and length data are listed on the righthand plots.

For sample SE5-1, the inclusion of the youngest 3 AHe grain age data into the QTQt thermal history modeling (Figure 9a) provides a much more precise ca. 20 Ma time for onset of rapid late Cenozoic cooling in this sample from temperatures of ca. 60-70 °C, compared to using the AFT data only (Figure 7c). Interestingly, HeFTy modeling results using AFT and AHe data from this sample, while only successful when using the two youngest AHe grain ages, show very similar results with acceptable fit paths indicating the onset of rapid cooling between ca. 20 and

15 Ma (Supplemental Figure S2). For sample SE5-1, two anomalously older grain ages that show no relationship with higher eU or grain size were excluded from the modeling as these older ages likely reflect helium implantation effects (Murray et al. 2014).

For sample LM8B, all 5 AHe grains ages and the AFT data are predicted well by the most-likely expected model thermal history (Figure 9b). However, in this case, any improvements in the constraints to the thermal history by including the AHe data relative to just using the AFT data (Figure 5d) are less clear. The data are consistent with gradual, slow cooling throughout the Cenozoic, with any increase in late Cenozoic cooling not being well-resolved. The inverse thermal modeling results from HeFTy using the AFT data and the youngest two AHe grain ages (Supplemental Figure S2) show a majority of good fit paths that hint at the onset of more rapid cooling at around 20 Ma.

To convert the thermal histories into estimates of exhumation we use a geothermal gradient of 20-30 °C/km for the region (Ninju et al., 2019). Our results suggest that the footwall blocks of the southern Malawi Rift have undergone a rapid exhumation of up to about 2 km within the last 20 Ma. The Thyolo fault of the Shire Rift also shows indications that it has accumulated strain in terms of exhumation related to footwall uplift in the last 20-25 Ma of a magnitude of about 2 km. This further solidifies our observations from fault geometry, and regional cooling age analysis, which all point towards rift linkage and transfer of strain across the accommodation zone between these rift systems of different origins.

4.5 Remote Sensing Analysis

The results of the analysis carried out on a 30-m resolution SRTM-DEM using QGIS and ENVI software to map major fault systems of the study area are shown in Figures 10 and 11. Slope analysis (Figure 10) and SRTM-DEM hillshade maps (Figure 11) of the study area show fault systems along the interaction zone between the Malawi Rift and the Shire Rift. The mapped faults show a pattern/model of rift linkage (Kolawole et al., 2021; Brune et al., 2017) whereby the potential for strain transfer can be interpreted and inferred from the geometry.

The density plot of the fault networks along the Southern Malawi Rift and Shire Rift show a higher density of the mapped faults from the Malawi active fault database across the Zomba Graben. This zone of high faults network density also shows faults of varyingFaults can be divided into three zones based on fault densities and their orientations of the major trend of the fault strikes (NNE – SSW & SW - NE) which makes it distinct from(Fig. 11). In the Southern Malawi Rift (Rfit Zone, faults strike NW-SE to N-S (trending 310°-010°). In the Shire Rift the faults are mostly oriented NW-SE (trending 290°-335°). In the rift interaction zone, the faults strike NNW-SSE). to NNE-SSW (trending 340°-035°) and the fault density is the highest. The results of the faults network density plot highlight the Southern Malawi rift zone, the Shire Rift zone, and what we now suggest to be the rift interaction zone between the two rift systems (Figure 11).

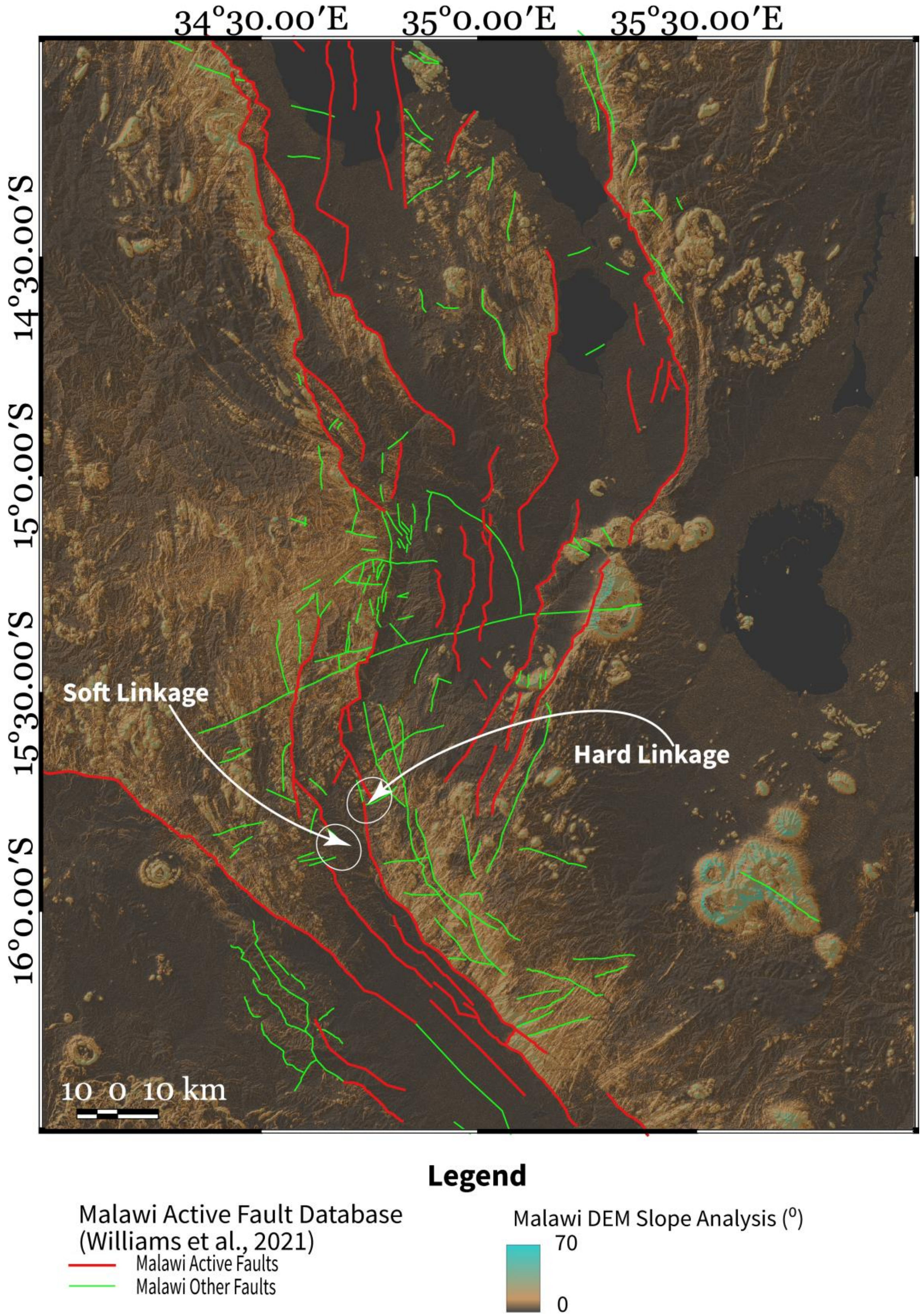
34°30.00′E
35°0.00′E
35°30.00′E
14°30.00′S
15°0.00′S
15°30.00′S
16°0.00′S
Soft Linkage
Hard Linkage
10 0 10 km
Legend
Malawi Active Fault Database
(Williams et al., 2021)
Malawi Active Faults
Malawi Other Faults
Malawi DEM Slope Analysis (°)
70
0

565

Figure 10: Slope analysis map overlain by some of the fault systems mapped across the accommodation zone between the southern Malawi Rift and Shire Rift (Modified after Kolawole et al., 2021). The white arrows and ellipses show examples of what we considered as soft or hard linkages between faults.

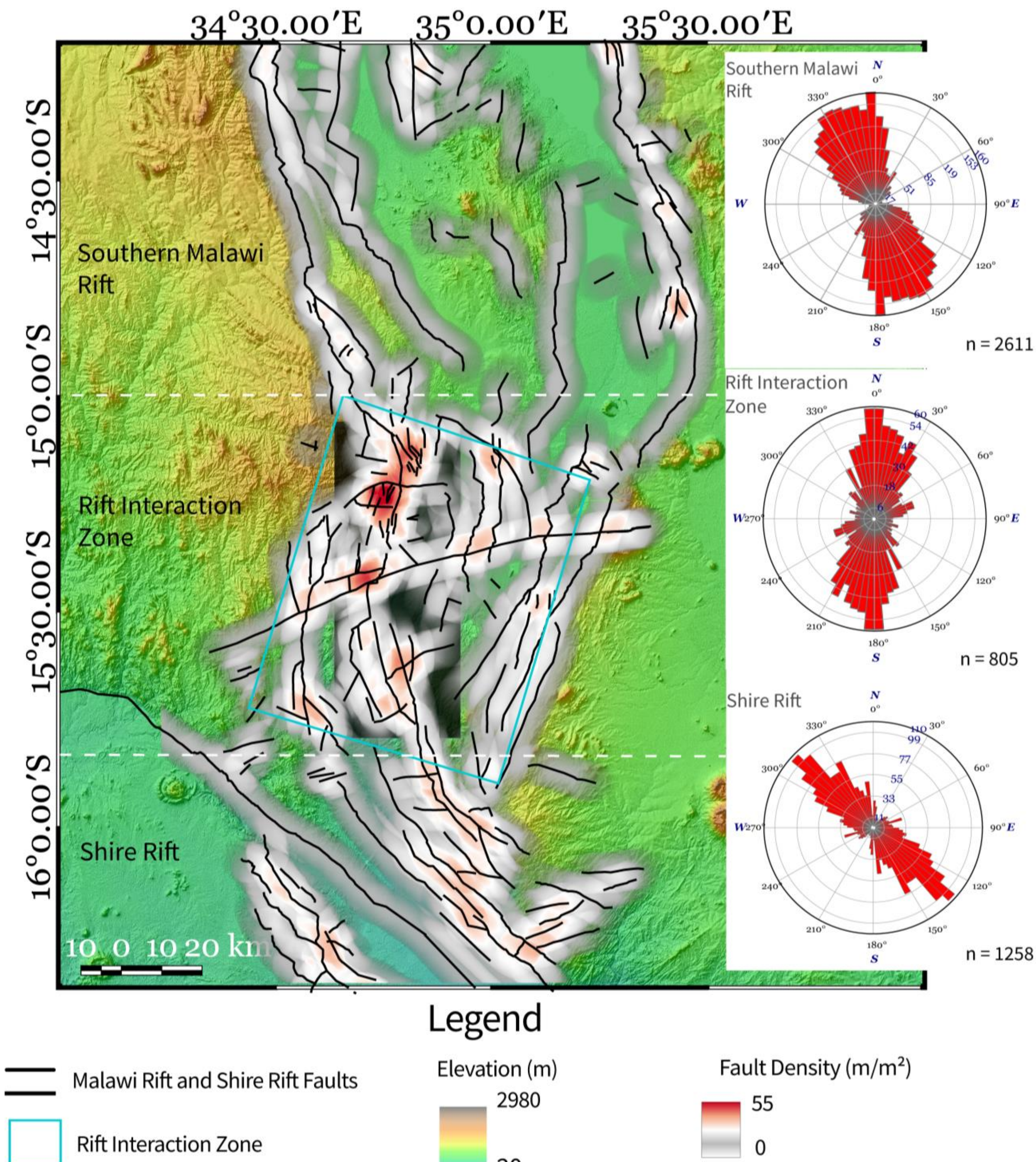

Figure 11: Hillshade map overlain by some of the fault systems mapped and the respective density plots of the fractures across the rift interaction zone between the southern Malawi Rift

and Shire Rift. The black background within the rift interaction zone highlights region where most of the rift interctions are concentrated.

4.6 Strain Rates

Using equations (1) and (2) (see Section 3.4 above) strain rates were estimated using maximum footwall uplift and exhumation amounts as the throw of the faults based on the new thermochronological data, and estimates of fault displacement and geometry based on the remote sensing analysis acquired in this study. Table 4 shows results from the southern Malawi Rift and estimates based on previous studies along the Livingstone Fault bordering the northern Malawi Rift (Van Der Beek et al., 1998; Mortimer et al., 2016; Accardo et al., 2018).

The results show extension rates to vary from 0.03 to 0.10 mm/yr and the slip rates to vary from 0.10 to 0.14 mm/yr for the southern Malawi Rift. The extension and slip rates are lower than those calculated for the Livingstone Fault in the northern Malawi Rift.

Table 4: Strain rate estimates across the southern Malawi Rift and northern Malawi Rift

	Uplift/Throw of Border Faults (km)	**Displacement (km)**			**Strain Rates**			
		Heave/Extension (km)			**Timing of Uplift (Ma)**	**20**		
Fault Dip		**45º**	**60º**	**75º**		**45º**	**60º**	**75º**
Southern Malawi Rift	2.00	2.83	2.31	2.07	Slip Rate (mm/yr)	0.14	0.12	0.10
		2.00	1.15	0.54	Extension Rate (mm/yr)	0.10	0.06	0.03
Northern Malawi Rift (Livingstone Fault)	6.40	9.05	7.39	6.63	Slip Rate (mm/yr)	0.45	0.37	0.33
		6.40	3.70	1.71	Extension Rate (mm/yr)	0.04	0.19	0.09

5 Discussion

5.1 Thermochronological Findings

The main finding from the low temperature thermochronologic data obtained in this study is that they show a Miocene cooling episode associated with footwall uplift and erosion of major extensional border faults associated with the southern Malawi Rift. Additionally, the new data reveal pre-Cenozoic cooling episodes from Cretaceous to early Permian suggesting include tectonic activities associated with Karoo Rifting (i.e. normal faulting and volcanism) during the Permian to Early Jurassic, to the formation of Cretaceous alkaline magmatic complexes (Castaing, 1991). The thermal histories of the samples along the border faults of Southern Malawi Rift and Shire Rift show some similarities and disparities in the various tectonic and thermal events that these two rift systems have undergone.

The thermochronologic modeling results from some of our samples also indicate a cooling event at around 70-80 Ma that is younger than the Chilwa alkaline magmatism. Similar cooling ages are quite common in the region. For example, Emmel et al. (2011; 2014) show widespread ca. 80 Ma AFT ages in Mozambique immediately east of our study area, but they provide no interpretation for its origin). Although a full understanding of the earlier pre-Cenozoic thermal history of southern Malawi is not the main focus of our study, and more work is merited to understand the cause of this late Cretaceous cooling, the localized nature of this event (e.g. seen in only 3 of 5 samples in the footwall of the Malombe Fault) leads us to speculate that it may reflect heating related to undated regional magmatism of this age or local resetting of samples by hot-fluid flow and/or mineralization at this time. Alternatively, similar 80-100 Ma AFT ages from the Chilwa Alkaline Province led Eby et al. (1995) to suggest this post-magmatic cooling was related to exhumation caused by localized uplift and doming, although no major tectonism of this age is known locally. However, major Late Cretaceous uplift is well documented in the South African plateau to the south (e.g. Said et al., 2015) and a major increase in Late Cretaceous sediment flux is documented in the delta of the Zambezi River that flows through the Shire Rift (Walford et al., 2005).

Data from previous thermochronological studies from across the Malawi Rift (Van Der Beek et al., 1998; Eby et al., 1995, Mortimer et al., 2016) allows for regional comparison of our new data to the wider dataset. A longitudinal comparison of AFT from the regional dataset shows similar ages for onset of Cenozoic exhumation at the northern and southern ends of the Malawi Rift. This observation does not support previous hypotheses stating that the initiation of rifting in the southern Malawi Rift is younger than in the northern Malawi Rift (Castaing et al., 1991; Daszinnies et al., 2008). Our results instead suggest a coeval onset model of Cenozoic rifting along the length of the Malawi Rift. Although cooling ages against distance along rift strike seem to show a trend of younger ages near the southern fault tips, suggesting the faults grew by lengthening of the fault towards the tip and a hybrid model of normal fault growth. Cooling and erosion of rift flanks are considered the leading cause of this age variation.

The thermal history modeling results for LM8B using the AHe data from all 5 grains in QTQt are not well-defined and seem to show steady cooling until the present day. We suggest that this is because the throw on the Malombe Fault is not enough to have exhumed footwall rocks from formerly well within the AHe partial retention zone (or AFT annealing zone) prior to the onset of faulting. Sample SE5-1, from the northern margin of the Shire Rift, shows that this fault was reactivated at ca. 20-15 Ma with a vertical footwall uplift of 50-70 °C equivalent (ca. 1-2 km). Our remote sensing analysis also shows this fault appears to show a hard linkage to the major east bounding fault of the southern Malawi Rift further supporting that late Cenozoic rifting and extensional strainextension along the southern Malawi Rift has propagated southward, and reactivated pre-existing older border faults of the Shire Rift in the last ca. 20 Ma.

Overall, the thermal history is tightly constrained with the onset of cooling at around 20 Ma from well-constrained temperatures of around 70°C (used in the estimation of the magnitude of uplift along the faults). This onset overlaps with the 23±3 Ma onset recorded by low-temperature thermochronologic data along the Livingstone Fault in the north in Mortimer et al., (2016). In summary, the thermal and geologic history records heating and post-magmatic cooling associated with alkaline igneous intrusions during the Cretaceous, followed by localized cooling and exhumation during the Late Cretaceous to early Cenozoic. Cenozoic East African Rift faulting and subsequent sediment deposition led to the burial of the basement rocks in the various basins formed. The thermal setting of a fault zone is likely controlled bya factors such as the regional geothermal structure and background thermal history of the study area, heating from friction along the wall rocks during faulting in the brittle regions, and heating of the wall rocks by hot fluid flow in and around the fault zone (Foster, 2019).

5.1.1 Malombe Fault

The Malombe Fault borders the eastern side of the Shire Horst at the southern end of the Malawi Rift (Figure 2). All five samples analyzed from the footwall of this fault (LM13, LM9, LM8B, LM7, and LM1) were from Precambrian gneisses. The Malombe Fault revealed three distinct cooling episodes during the Early Cretaceous, Late Cretaceous to early Cenozoic, and late Cenozoic. The Early Cretaceous cooling appears to be related to post-intrusion cooling following Cretaceous alkaline igneous intrusion in the southern Malawi Rift. The localized later Cretaceous cooling seen in 2 of the 5 samples we suspect is related to either localized heating and/or regional uplift and erosion. All samples then show steady minimal thermal change that preceded the East African rifting along the Malawi Rift. The third and final late Cenozoic cooling episode records activity along the faults of the Malawi Rift, reflecting rift initiation, erosion, and associated uplift/exhumation.

5.1.2 Zomba Fault and Chingale-step Fault

The 2 samples (Z16 and Z22) that were collected from the Chingale-step Fault footwall scarps of the Zomba Graben are a syenite and a slightly foliated granite close to the Chilwa Alkaline Igneous Province. The Late Cretaceous cooling ages obtained from these samples (consistent with AFT cooling ages of samples from the region published by Eby et al., 1995) record post-intrusion cooling. AFT ages typically record post-intrusion cooling events, but if the magma is intruded into the upper crust where host rocks are resident at temperatures cooler than the PAZ, the time spent between crystallization and the first retention of fission tracks is shorter than the resolution of the dating method (Jaeger 1968). The samples also record the 70-80 Ma cooling episode as also observed in some of the samples along the Malombe Fault, which we suggest might be due to esresetting of samples by undated regional magmatism, mineralization, and/or hydrothermal flow. Therefore, AFT ages from shallow igneous intrusions and volcanic rocks like the ones across the Chilwa Alkaline Province can be considered as close to their magmatic ages and thus give no direct constraint on magnitudes and rates of exhumation during the Late Cretaceous. This is consistent with the thermal modeling of these samples from their mean track length distributions.

5.1.3 Thyolo-Muona Fault

We collected and measured AFT cooling ages from 3 rock samples (Precambrian gneisses) from the Thyolo Fault (SE17 and SE18 1-2) and its synthetic fault (Muona Fault) south-east of it (SE5-1) along the northern margin of the Shire Rift, with additional exploratory AHe data collected from sample SE5-1. The two samples from the Thyolo Fault (SE 17 and SE 18 1-2) have Late Cretaceous-Paleocene cooling ages and the one from the Muona Fault (SE 5-1) has a Late Cretaceous (66 Ma) cooling age. The three distinct cooling episodes revealed by thermal modeling of these samples are similar to those recorded from the Malombe Fault and Chingale-step Fault of the southern Malawi Rift. This suggests the southern Malawi Rift and Shire Rift have experienced spatially correlated uplift and exhumation histories throughout the Cenozoic, with the two rift systems experiencing hard and soft linkages of their border faults. This is supported by spatial trends in thermochronological data and thermal history modeling, which display similar rates of cooling across the southern Malawi Rift and the Shire Rift.

5.1.4 Mwanza Fault

Three rock samples (SW2, SW7-1, and SW13) which include Precambrian gneisses and a felsic dyke were collected from the footwall fault scarps of the Mwanza Fault further west along the northern border of the Shire Rift. Sample SW13 produced the youngest AFT cooling age measured in this study. The other two samples (SW2 and SW13) have Late Cretaceous cooling ages. The young age from sample SW13 suggests that the Mwanza Fault has undergone Cenozoic cooling, even though the Shire Rift is believed to be as old as the Paleozoic-Mesozoic. The Cretaceous age recorded by SW7 is believed to be due to the proximity of the sample to coeval Cretaceous alkaline ring complexes south of the fault. These intrusions are responsible for a series of dikes in the region. Although the thermal modeling of these samples was not as well-constrained as our other samples, they still show similar thermal histories to samples from the Chingale-step Fault where the samples are also near (or sampled from) the Early Cretaceous alkaline ring complexes. Our result also suggests that the Mwanza Fault pre-dates the Thyolo Fault in the North-East of the Shire Rift.

5.2 Fault Pattern along the Accommodation Zone

The fault system observed from the hillshade map (Fig. 11) and slope analysis (Fig. 10) suggest soft and hard linkages between the southern Malawi Rift and the Shire Rift. The hillshade map was used to highlight the faults and joints between the two rift systems. The fault density plot (Fig. 11) also shows a high concentration of faults along the accommodation zone between the southern Malawi Rift and the Shire Rift. This result suggests the presence of fault systems capable of initiating strain transfer between the two linked rift systems.

The slope analysis map (Fig. 10) shows the variation of topographic slope along the border faults and also across the accommodation zone. Previous studies have investigated the relationship between relay ramps of various types (Fossen and Rotevatn, 2016; Peacock et al., 2002). Relay ramps that tend to link up by a breached fault have slopes that range from 10-15^{o} at the onset of breaching (Fossen and Rotevatn, 2016). Relay ramps also demonstrate that the accommodation zone becomes steeper downwards as strain increases and becomes breached; the maximum dip of the ramp reaches around 13–14^{o} (Giba et al. 2012). This is observable in Figure 9 as the accommodation zone between the two rift systems is characterized by various fault systems and ramps that exhibit slopes ranging from about 10-15^{o}.

The fault density plot (Fig. 11) generated along the Malawi Rift and the Shire Rift also shows a high concentration of faults in terms of length and number of faults over a specific area within the accommodation zone between the two rift systems. This suggests recent interaction in terms of strain accommodation and transfer between the southern Malawi Rift and the Shire Rift. The density map also shows a higher density of faults at the southernmost part of the Malawi Rift which indicates that this region is undergoing Rift linkage. The zone of linkage and high fault density also coincides with the zone described by Kolawole et al., (2021) as a rift interaction zone (overlapping oblique rift interaction zones). The study by Kolawole et al. (2021) suggests that this rift interaction has recently been breached, which is consistent with the results of this study in terms of ages of tectonic uplift across the two rift systems, geometry, and lack of sedimentary cover over the zone of interaction.

5.3 Strain Rates: Southern Malawi Rift vs Northern Malawi Rift

The results of the strain rate calculations from this study show a difference in the strain rates across the northern Malawi Rift compared with those of the southern Malawi Rift. This result, combined with our thermochronological findings that suggests a coeval opening of the Malawi Rift, supports a decreasing rate of strain accommodation from the northern segment of the rift to the southern segment. This new data contradicts the consensus of a younger southern Malawi Rift compared to the northern Malawi Rift based on the varying sedimentary fill, and pattern and magnitude of strain accommodation (Specht and Rosendahl, 1989). We suggest this disparity is due to varying rates of strain accommodation and not the ages of initiation as earlier proposed. The northern Malawi Rift seems to be accommodating strain faster than the southern Malawi Rift. This could be due to several reasons which include but are not limited to the southern location of the Euler pole of rotation responsible for the movement of the Rovuma and Nubian plates (Saria et al. 2013), the changes in lithology and rheology across the rift (see Figure 1 for reference), and the proximity to other geologic structures (like the older Shire Rift) that can contribute to the inhibition, arrest, or termination of strain accommodation across the southern Malawi Rift (Kim and Sanderson, 2002; Bergen and Shaw, 2010).

Previous studies like Williams et al. (2021) have attempted to estimate the rate of strain accommodation along the border and intra-rift faults across the southern Malawi Rift using slip rate estimation from earthquake data. Slip rates estimated for the southern Malawi Rift from the study range from 0.08 to 0.5 mm/yr. Stamps et al., (2018) investigated the strain rate across the entire EARS using geodetic estimation of the motion along the moving plates. Our estimation of strain rates for the Northern Malawi Rift is consistent with their calculations for the region. Their study showed that Northern Malawi is one of the places with a high strain rate magnitude which could be as high as 2 mm/yr. Stamps et al., (2008) also estimated the extension rate, which is the cumulative crustal extension between the two plates rifting apart along the Malawi Rift to be 2.2 mm/yr in the northern Malawi Rift and 1.5 mm/yr for the southern Malawi Rift. The results of these studies (Williams et al., 2021; Stamps et al., 2021; 2018; 2008) compared with the results of our strain rate estimations support that rifting across the southern Malawi Rift initiated in late Oligocene–early Miocene (~25-20 Ma) just as the Northern Malawi Rift, but that a larger percentage of the strain accommodation did not start accumulating until closer to the late Miocene (~10-5.3 Ma). Even though Mortimer et al. (2016) estimated the onset of rifting at 23

Ma, thermal modeling of their (U-Th)/He data shows most of their rapid cooling episodes starting at about ~10 Ma. Their range of onset of rapid cooling associated with rifting and similar results from AFT dating presented in Van Der Beek et al. (1998) varies from 25 Ma to less than 10 Ma, further supporting the similarities between our results and those from further north suggesting coeval onset and changes in strain rates in the northern and southern parts of the Malawi Rift.

5.4 Coeval Rift Model across the Malawi Rift

The results of this study from low-temperature thermochronology thermal modeling and strain rate estimations suggest a coeval onset of the Cenozoic rifting along the full length of the Malawi Rift. We propose a model that explains how strain has been accommodated across a coeval Malawi Rift since its initiation illustrated in Fig. 12. In this model, the Malawi Rift was initiated as isolated faults along the entire length of the incipient rift during the Miocene (Figure 11a). These isolated border faults were connected by soft overlapping linkages. Following initiation of these isolated normal faults, the faults then grew by lengthening, linkage, and segmentation into larger border faults and intra-rift faults by a hybrid model of fault growth with alternating phases of lengthening and accrual of displacement to accommodate the cumulative strains along the faults and across the rift as manifested in the observed present-day architecture of the Malawi Rift (Fig. 12b).

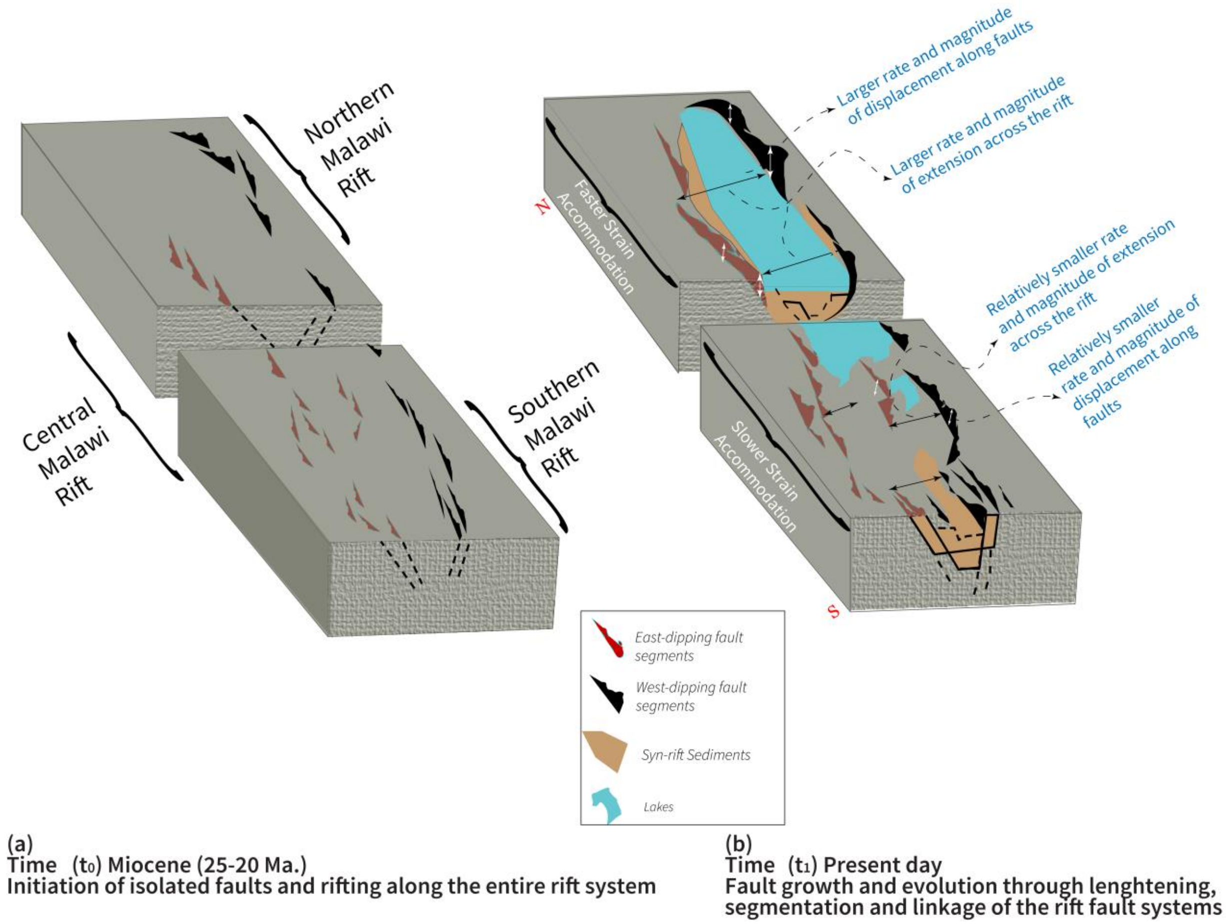

Figure 12: Conceptual model showing the evolution of the Malawi Rift in terms of strain accommodation from initiation. (a) Coeval initiation of isolated faults across the rift segments. Some of the faults overlap by soft linkages. (b) Present-day architecture of the rift. It shows the isolated faults have coalesced by hard linkage in the north at a rate greater than the magnitude of strain accommodation in the south which has isolated faults that have grown and linked by hard linkage and more soft linkages at a slower rate compared to the northern Malawi Rift.

5.4 Implications for the history of the East African Rift

The results presented here suggest the southern Malawi Rift was initiated in the early Miocene, just like the northern Malawi Rift (Fig. 11). This interpretation differs from earlier studies, where active rifting across the Western Branch of the EARS has been proposed to have been initiated at 8 - 7 Ma (Ebinger, 1989; Morley and Ngenoh, 1999) and 23 Ma (Mortimer et al., 2016), which is later than in the Eastern Branch of the EARS where rifting began in the

Eocene (Morley and Ngenoh, 1999). Similar studies across the Eastern Branch have also highlighted cooling episodes in the Late Cretaceous–Paleocene and late Miocene–Pliocene (Foster and Gleadow, 1996; Spiegel et al., 2007), which were also recorded by previous thermochronological studies from the northern parts of the Western Branch that outline the onset of cooling in thermal models in the Eocene (50 Ma–40 Ma; Van der Beek et al., 1998; Bauer et al., 2010). Stratigraphic studies and the detrital geochronology of sediment from the Rukwa Rift Basin, in the southern Western Branch, suggest active rifting began in the Oligocene (Roberts et al., 2012) implying uplift of the landscape may have started even earlier and is consistent with the timing of rift initiation from thermochronological work in the Eastern Branch (Boone et al., 2019; Jess et al 2019).

The underlying mechanism that formed the EARS remains a debated topic, with both passive and active mechanisms postulated in various studies (Chorowicz, 2005). The focal planes of earthquakes that are parallel to Miocene escarpments (Shudofsky, 1985) and volcanic provinces along faults aligned subparallel to border-fault systems indicate rifting has been active episodically throughout the history of their respective basins (Ebinger, 1989; Ebinger and others, 1989). North-south propagation of rifting systems has been suggested for the Western Branch of the rift system based on geomorphological evidence, just as the observed regional north-south age progression of volcanic activity recognized in the Kenya rift (Capart, 1949; Haldemann, 1969; Shackleton, 1978; Crossley and Crow, 1980; Williams and Chapman, 1986; Bosworth, 1987). However, the timing of faulting and rifting in general in many parts of the Western rift system is poorly constrained. Additional age constraints are needed to evaluate the trend of volcanic flows along the western branch as the volcanic intrusions from the Rungwe province (the southernmost Western rift volcanic province) which are approximately 3 Ma older than flows in the northern part of the Western rift and this contradicts the southward propagation of the Western Branch (Jess et al., 2019). Also, thermochronological constraints from the onset of rifting and timing of faulting from this study and previous studies (e.g. Jess et al., 2019; Mortimer et al., 2016; Van Der Beek et al., 1998) along the Western Branch do not fully support a southward propagation of the rift systems. However, this does not imply that the growth model of individual major rift bounding faults of the segmented rift basins does not occur by fault propagation. Instead, our results simply identify a coeval initiation of rifting processes across the entire length of the Malawi Rift. We suggest that even though rifting is initiated at the same time in the northern and southern end of the Malawi Rift, the differences in structures along this early-stage rift used as proxies for the magnitude of strain being accommodated is due to the alternating phase lengthening and displacement of fault accrual in the normal fault growth model of the Malawi Rift (Ojo et al., 2022; Pan et al., 2022).

Our results unite the two ends of the Malawi Rift temporally and provide the means for generating a unique mechanism for the formation of the entire rift system. Though this study does not provide greater insight into a wider mechanism of rift formation, it supports the notion of coeval onset of rifting along the whole length of the Malawi Rift and subsequently most parts of the Western Branch of EARS in the Miocene which correlates to numerous tectonic processes including rifting phases in Northern Kenya and Sudan (Bosworth, 1992; Morley et al., 1992), kinematic changes across the Indian Ocean (Cande et al., 2010), and the broader collision of African into Eurasia (Rosenbaum et al., 2002). Our results also highlight the need for further studies of sediment fill within rift and rocks along the fault scarp using methods other low-temperature thermochronological methods like the apatite (U-Th)/He data, to determine more precisely the timing of extensional onset and erosional history of the basins. The results of this work alongside previous studies suggest coeval strain accommodation of the Western Branch of the East African Rift and thus, the modern consensus on rift initiation requires review.

6 Conclusions

Apatite fission-track analysis, apatite (U-Th)/He dating, thermal history modeling, and fault geometry from remote sensing analysis suggest the Southern Malawi Rift initiated in the Miocene and has continued to grow and evolve through multiple phases of gradual and linear uplift. Our results support that the border faults of the southern Malawi Rift and Shire Rift have experienced spatially correlated uplift and exhumation histories throughout the Cenozoic, with the two rift systems experiencing hard and soft linkages of these border faults. This is supported by spatial trends in thermochronological data and thermal history modeling, which display similar rates of cooling across the southern Malawi Rift and the Shire Rift. The similarities in the thermal history of the faults along the southern Malawi Rift (Malombe Fault and Chingale Step Fault) with the Thyolo Fault along SE of the Shire Rift indicate that these two rift systems have linked up along this axis. This is confirmed by the remote analyses and characterization of the fault systems. The remote sensing analysis also shows faults and other fault systems along the accommodation or transfer zone between the Malawi Rift and Shire Rift (Thyolo Fault) that could be responsible for strain accommodation and transfer but little to none between the Mwanza Fault and the Malawi Rift.

Even though the Shire Rift is a relic of an older rifting process that predated the East African Rift System (EARS), this study reveals that these two distinct rift systems are now linked, and strain is being transferred from the Malawi Rift that reactivated the Shire Rift in the late Cenozoic. This study indicates that the border faults along the northern flank of the Shire Rift have accumulated about 1-2 km of relative vertical footwall uplift since the late Miocene. This is also consistent with the height of the present-day scarp that can be observed along the Thyolo Fault.

The timing of rift initiation in the southern Malawi Rift estimated in this study appears to be about the same range as that estimated by previous studies for the northern Malawi Rift (Van Der Beek et al., 1998; Mortimer et al., 2016). This supports that rifting in the northern and southern Malawi Rift began at about the same time and that differences in the rate of strain accumulation are responsible for the disparity in throw and displacement estimation along these sections of the Malawi Rift. Our conclusion is also supported by the GPS results in Stamps et al. (2021) which show slower cumulative strain rates along the diverging plates similar to our individual border fault estimations along the Malawi Rift in the south compared to the north.

These results have broad implications for the rifting history of the Western Branch of the EAR, implying rift initiation began in the Miocene across the entire western branch and subsequent difference in the rate of strain accommodation along each rift system is responsible for the apparent southward trend of propagation along the rift system.

Acknowledgments, Samples, and Data

This work was supported by the Geological Society of America (GSA) Awards for Geochronology Student Research2 (AGeS2) program. AGeS2 is supported by NSF EAR-1759200, -1759353, -1759201 awards to R.M. Flowers (CU-Boulder), J.R. Arrowsmith (ASU), and V. McConnell (GSA). Samples were collected under the support of NSF II-1358150. We thank the Fission Track Laboratory at the University of Arizona for their collaboration to make the execution of this project possible, ZirChron LLC for the mineral separation of the rock samples, and the Oregon State University Radiation Center facility for sample irradiation. Data supporting the conclusions can be found in the cited references, in the Supporting Information provided as supplements and will also be made available through the PANGAEA Data Publisher for Earth & Environmental Science (link to the repository will be provided as soon as the data become published). This is Oklahoma State University Boone Pickens School of Geology contribution 2022-XX.

References

Abbate, E., & Sagri, M. (1980). Volcanites of Ethiopian and Somali Plateaus and major tectonic lines. Atti Convegni Lincei, 47, 219-227.

Armijo, R., Tapponnier, P. & Mercier, J. 1986 Quaternary extension in southern Tibet: field observations and tectonic implications. J. Geophys. Res. 91, 13 803–13 872

Bell, R. E., Jackson, C. A.-L., Whipp, P. S., and Clements, B. (2014), Strain migration during multiphase extension: Observations from the northern North Sea, Tectonics, 33, 1936–1963, doi:10.1002/2014TC003551.

Bloomfield, K. (1965). The geology of the Middle Shire Hydro-Electric Power Sites in Records of the Geological Survey of Malawi VII, 29–44. *Government Printer, Zomba, Malawi*.

Bonini, M., Corti, G., Innocenti, F., Manetti, P., Mazzarini, F., Abebe, T., and Pecskay, Z. (2005), Evolution of the Main Ethiopian Rift in the frame of Afar and Kenya rifts propagation, Tectonics, 24, TC1007, doi:10.1029/2004TC001680.

Brichau, S., Ring, U., Ketcham, R. A., Carter, A., Stockli, D., & Brunel, M. (2006). Constraining the long-term evolution of the slip rate for a major extensional fault system in the central Aegean, Greece, using thermochronology. Earth and Planetary Science Letters, 241(1-2), 293-306.

Brun, J.-P. & Choukroune, P. (1983). Normal faulting, block tilting and decollement in a stretched crust. Tectonics 2, 345–356.

Brune, S., Corti, G., and Ranalli, G. (2017), Controls of inherited lithospheric heterogeneity on rift linkage: Numerical and analog models of interaction between the Kenyan and Ethiopian rifts across the Turkana depression, Tectonics, 36, 1767– 1786, doi:10.1002/2017TC004739.

Buck, R. W. (1991) Modes of continental lithospheric extension. J. Geophys. Res. 96, 20 161–20 178.

Calais, E., d'Oreye, N., Albaric, J. et al. (2008). Strain accommodation by slow slip and dyking in a youthful continental rift, East Africa. Nature 456, 783–787 https://doi.org/10.1038/nature07478

Carrapa, B., (2010), Resolving tectonic problems by dating detrital minerals: Geology, v. 38, p. 191–192.

Carrapa, B., S. Bywater-Reyes, P. G. DeCelles, E. Mortimer, and G. E. Gehrels, (2011), Late Eocene–Pliocene basin evolution in the Eastern Cordillera of northwestern Argentina (25°–26°S): regional implications for Andean orogenic wedge development: Basin Research.

Carter, A., & Gallagher, K. (2004). Characterizing the significance of provenance on the inference of thermal history models from apatite fission-track data-a synthetic data study. Special Papers-Geological Society of America, 7-24.

Carter, A., & Foster, G. L. (2006). Enhanced source characterisation through combined FT and Sm–Nd on single detrital apatites. Geochimica et Cosmochimica Acta, 18(70), A86.

Castaing, C. (1991). Post-Pan-African tectonic evolution of South Malawi in relation to the Karroo and recent East African rift systems. Tectonophysics, 191(1–2), 55–73. https://doi.org/10.1016/0040-1951(91)90232-H

Coney, P. J. & Harms, T. A. (1984) Cordilleran metamorphic core complexes: Cenozoic extensional relics of Mesozoic compression. Geology 12, 550–554.

Corti, G. (2009). Continental rift evolution: from rift initiation to incipient break-up in the Main Ethiopian Rift, East Africa. Earth-science reviews, 96(1-2), 1-53.

Cowie, P. A., Underhill, J. R., Behn, M. D., Lin, J., & Gill, C. E. (2005). Spatio-temporal evolution of strain accumulation derived from multi-scale observations of Late Jurassic rifting in the northern North Sea: A critical test of models for lithospheric extension. Earth and Planetary Science Letters, 234(3-4), 401-419.

Craig, T.J., Jackson, J.A., Priestley, K., and Mckenzie, D., (2011), Earthquake distribution patterns in Africa: Their relationship to variations in lithospheric and geological structure, and their rheological implications: Geophysical Journal International, v. 185, p. 403–434, https://doi.org/10.1111/j.1365-246X.2011.04950.x.

Daszinnies, Matthias & Emmel, Benjamin & Jacobs, Joachim & Grantham, Geoff & Thomas, Bob. (2008). Denudation In Southern Malawi and Northern Mozambique: Indications of the Long-term Tectonic Segmentation of East Africa During the Gondwana Break-up.

Daszinnies, M.C., Jacobs, J., Wartho, J.A., and Grantham, G.H., 2009, Post Pan-African thermo-tectonic evolution of the north Mozambican basement and its implication for the Gondwana rifting. Inferences from $^{40}Ar/^{39}Ar$ hornblende, biotite and titanite fission-track dating: Geological Society, London, Special Publications, v. 324, p. 261–286, doi:10.1144/SP324.18.

Deeken, A., E. R. Sobel, I. Coutand, M. Haschke, U. Riller, and M. R. Strecker, (2006), Development of the southern Eastern Cordillera, NW Argentina, constrained by apatite fission track thermochronology: from early Cretaceous extension to middle Miocene shortening: Tectonics, v. 25.

Deng, H., Ren, J., Pang, X., Rey, P. F., McClay, K. R., Watkinson, I. M., ... & Luo, P. (2020). South China Sea documents the transition from wide continental rift to continental break up. Nature Communications, 11(1), 1-9. https://doi.org/10.1038/s41467-020-18448-y

Ebinger, C. J., Deino, A. L., Drake, R. E., & Tesha, A. L. (1989). Chronology of volcanism and rift basin propagation: Rungwe volcanic province, East Africa. Journal of Geophysical Research, 94(B11). https://doi.org/10.1029/jb094ib11p15785

Ebinger, C. (2005). Continental break-up: the East African perspective. Astronomy & Geophysics, 46(2), 2-16.

Ebinger, C., & Scholz, C. A. (2011). Continental rift basins: the East African perspective. Tectonics of sedimentary basins: Recent advances, 183-208.

Ebinger, C.J., Oliva, S.J., Pham, T-Q., Peterson, K., Chindandali, P., Illsley-Kemp, F., Drooff, C.,

Eby, G. N., Roden-Tice, M., Krueger, H. L., Ewing, W., Faxon, E. H., & Woolley, A. R. (1995). Geochronology and cooling history of the northern part of the Chilwa Alkaline Province, Malawi. Journal of African Earth Sciences, 20(3–4), 275–288. https://doi.org/10.1016/0899-5362(95)00054-W

Emmel, B., Kumar, R., Ueda, K., Jacobs, J., Daszinnies, M.C., Thomas, R.J., and Matola, R., 2011, Thermochronological history of an orogen-passive margin system: An example from northern Mozambique: Tectonics, v. 30, p. TC2002, doi:10.1029/2010TC002714.

Emmel, B., Kumar, R., Jacobs, J., Ueda, K., Van Zuilen, M., and Matola, R., 2014, The low-temperature thermochronological record of sedimentary rocks from the central Rovuma Basin (N Mozambique) — Constraints on provenance and thermal history: Gondwana Research, v. 25, p. 1216–1229, doi:10.1016/j.gr.2013.05.008.

England, P., and Molnar, P., 1990, Surface Uplift, Uplift of Rocks, and Exhumation of Rocks: Geology, v. 18, p. 1173–1177.

Faulds, J. E., & Varga, R. J. (1998). The role of accommodation zones and transfer zones in the regional segmentation of extended terranes. Geological Society of America Special Papers, 323, 1-45.

Flannery, J. W., & Rosendahl, B. R. (1990). The seismic stratigraphy of Lake Malawi, Africa: implications for interpreting geological processes in lacustrine rifts. Journal of African Earth Sciences, 10(3), 519–548. https://doi.org/10.1016/0899-5362(90)90104-M

Fitzgerald, P. G., Duebendorfer, E. M., Faulds, J. E., & O'Sullivan, P. (2009). South Virgin–White Hills detachment fault system of SE Nevada and NW Arizona: Applying apatite fission track thermochronology to constrain the tectonic evolution of a major continental detachment fault. Tectonics, 28(2).

Fossen, H., & Rotevatn, A. (2016). Fault linkage and relay structures in extensional settings—A review. *Earth-Science Reviews, 154*, 14-28.

Foster, A.N., and Jackson, J.A., (1998), Source parameters of large African earthquakes: Implications for crustal rheology and regional kinematics: Geophysical Journal International, https://doi.org/10.1046/j.1365-246x.1998.00568.x.

Foster D.A. (2019) Fission-Track Thermochronology in Structural Geology and Tectonic Studies. In: Malusà M., Fitzgerald P. (eds) Fission-Track Thermochronology and its Application to Geology. Springer Textbooks in Earth Sciences, Geography, and Environment. Springer, Cham. https://doi.org/10.1007/978-3-319-89421-8_11

Furman, T., Bryce, J. G., Karson, J., & Iotti, A. (2004). East African Rift System (EARS) plume structure: insights from Quaternary mafic lavas of Turkana, Kenya. Journal of Petrology, 45(5), 1069-1088.

Gallagher, K., Hawkesworth, C. J., & Mantovani, M. S. M. (1995). Denudation, fission track analysis and the long-term evolution of passive margin topography: application to the southeast Brazilian margin. Journal of South American Earth Sciences, 8(1), 65-77.

Gallagher, K., and Brown, R., 1997, The onshore record of passive margin evolution: Journal of The Geological Society, v. 154, p. 451–457.

Gallagher, K., Brown, R.W., and Johnson, C., 1998, Fission Track Analysis and its Application to Geological Problems: Annual Reviews in Earth and Planetary Sciences, v. 26, p. 519–572.

Gleadow, A.J.W., Duddy, I.R., Green, P.F., and Lovering, J.F., 1986, Confined fission track lengths in apatite: a diagnostic tool for thermal history analysis: Contributions to Mineralogy and Petrology, v. 94, p. 405–415.

Goldsworthy, M., & Jackson, J. (2001). Migration of activity within normal fault systems: examples from the Quaternary of mainland Greece. Journal of Structural Geology, 23(2-3), 489-506.

Green, P.F., 1986, On the Thermo-Tectonic Evolution of Northern England - Evidence from Fission-Track Analysis: Geological Magazine, v. 123, p. 493–506.

Hurford, A. J., and Green, P. F. (1983). The Zeta-Age Calibration of Fission-Track Dating. Isotope Geoscience, v. 1, p. 285-317.

Hey, R. (1977). A new class of "pseudofaults" and their bearing on plate tectonics: A propagating rift model. Earth and Planetary Science Letters, 37(2), 321-325.

Ketcham, R.A., Carter, A., Donelick, R.A., Barbarand, J., and Hurford, A.J., 2007, Improved modeling of fission-track annealing in apatite: American Mineralogist, v. 92, p. 799–810, doi:10.2138/am.2007.2281.

Ketcham, R.A., Gautheron, C., and Tassan-Got, L., 2011, Accounting for long alpha-particle stopping distances in (U-Th-Sm)/He geochronology: Refinement of the baseline case: Geochimica et Cosmochimica Acta, v. 75, p. 7779–7791, doi:10.1016/j.gca.2011.10.011.

Kim, Y. S., Peacock, D. C., & Sanderson, D. J. (2004). Fault damage zones. Journal of structural geology, 26(3), 503-517.

Kolawole, F., Firkins, M. C., Al Wahaibi, T. S., Atekwana, E. A., & Soreghan, M. J. (2021). Rift Transfer Zones and the Stages of Rift Linkage in Active Segmented Continental Rift Systems.

Laó-Dávila, D. A., Al-Salmi, H. S., Abdelsalam, M. G., & Atekwana, E. A. (2015). Hierarchical segmentation of the Malawi Rift: The influence of inherited lithospheric heterogeneity and kinematics in the evolution of continental rifts. Tectonics, 34(12), 2399–2417. https://doi.org/10.1002/2015TC003953

Lavier, L. L., & Manatschal, G. (2006). A mechanism to thin the continental lithosphere at magma-poor margins. Nature, 440(7082), 324-328.

Lutz, T.M., and Omar, G.I., (1991), Inverse methods of modeling thermal histories from apatite fission-track data, Earth Planet. Sci. Lett., v. 104, p. 181-195

Macgregor, D., (2015), History of the development of the East African Rift System: A series of interpreted maps through time: Journal of African Earth Sciences, v. 101, p. 232–252, https://doi.org/10.1016/j.jafrearsci.2014.09.016.

Mahatsente, R., Jentzsch, G., & Jahr, T. (1999). Crustal structure of the Main Ethiopian Rift from gravity data: 3-dimensional modeling. Tectonophysics, 313(4), 363-382.

Maguire, P. K. H., Ebinger, C. J., Stuart, G. W., Mackenzie, G. D., Whaler, K. A., Kendall, J. M., ... & Harder, S. (2003). Geophysical project in Ethiopia studies continental breakup. EOS, Transactions American Geophysical Union, 84(35), 337-343.

Morley, C. K., Nelson, R. A., Patton, T. L., & Munn, S. G. (1990). Transfer zones in the East African rift system and their relevance to hydrocarbon exploration in rifts. AAPG bulletin, 74(8), 1234-1253.

Morley, C. K. (1999). Patterns of displacement along large normal faults: implications for basin evolution and fault propagation, based on examples from East Africa. AAPG bulletin, 83(4), 613-634.

Mortimer, E., Kirstein, L. A., Stuart, F. M., & Strecker, M. R. (2016). Spatio-temporal trends in normal-fault segmentation recorded by low-temperature thermochronology: Livingstone fault scarp, Malawi Rift, East African Rift System. Earth and Planetary Science Letters, 455, p. 62–72. https://doi.org/10.1016/j.epsl.2016.08.040

Muirhead, J. D., Kattenhorn, S. A., Lee, H., Mana, S., Turrin, B. D., Fischer, T. P., ... & Stamps, D. S. (2016). Evolution of upper crustal faulting assisted by magmatic volatile release during early-stage continental rift development in the East African Rift. Geosphere, 12(6), 1670-1700.

Muirhead, J. D., Wright, L. J., & Scholz, C. A. (2019). Rift evolution in regions of low magma input in East Africa. Earth and Planetary Science Letters, 506, 332-346.

Murray, K.E., Orme, D.A., & Reiners, P.W., 2014, Effects of U–Th-rich grain boundary phases on apatite helium ages: Chemical Geology, 390, 135–151, doi:10.1016/j.chemgeo.2014.09.023.

Nixon, C. W., McNeill, L. C., Bull, J. M., Bell, R. E., Gawthorpe, R. L., Henstock, T. J., ... & Ferentinos, G. (2016). Rapid spatiotemporal variations in rift structure during development of the Corinth Rift, central Greece. Tectonics, 35(5), 1225-1248.

Njinju, E. A., Kolawole, F., Atekwana, E. A., Stamps, D. S., Atekwana, E. A., Abdelsalam, M. G., & Mickus, K. L. (2019). Terrestrial heat flow in the Malawi Rifted Zone, East Africa: Implications for tectono-thermal inheritance in continental rift basins. *Journal of Volcanology and Geothermal Research*, *387*, 106656.

Péron-Pinvidic, G., & Manatschal, G. (2009). The final rifting evolution at deep magma-poor passive margins from Iberia-Newfoundland: a new point of view. International Journal of Earth Sciences, 98(7), 1581-1597.

Peyton S. L., Carrapa B., (2013), An introduction to low-temperature thermochronologic techniques, methodology, and applications, in C. Knight and J. Cuzella, eds., Application of structural methods to Rocky Mountain hydrocarbon exploration and development: AAPG Studies in Geology 65, p. 15–36.

Raab, M. J., Brown, R. W., Gallagher, K., Weber, K., & Gleadow, A. J. W. (2005). Denudational and thermal history of the Early Cretaceous Brandberg and Okenyenya igneous complexes on Namibia's Atlantic passive margin. Tectonics, 24(3), https://doi.org/10.1029/2004TC001688

Raab, Matthias J., Brown, R. W., Gallagher, K., Carter, A., & Weber, K. (2002). Late Cretaceous reactivation of major crustal shear zones in northern Namibia: Constraints from apatite fission track analysis. Tectonophysics, 349(1–4), 75–92. https://doi.org/10.1016/S0040-1951(02)00047-1

Reiners, P.W., Ehlers, T.A., and Zeitler, P.K., 2005, Past, present, and future of thermochronology: Reviews in Mineralogy and Geochemistry, v. 58, p. 1–18, doi:10.2138/rmg.2005.58.1.

Reiners, P.W., and Brandon, M.T., 2006, Using thermochronology to understand orogenic erosion: Annual Reviews in Earth and Planetary Sciences, v. 34, p. 419–466, doi:10.1146/annurev.earth.34.031405.125202.

Ring, U., Betzler, C., & Delvaux, D. (1992). Normal vs. strike-slip faulting during rift development in East Africa: the Malawi Rift. Geology, 20(11), 1015-1018.

Rosendahl, B. R. (1987). Architecture of continental rifts with special reference to East Africa. Annual Review of Earth and Planetary Sciences, 15, 445.

Said, A., Moder, C., Clark, S., and Ghorbal, B., 2015, Cretaceous–Cenozoic sedimentary budgets of the Southern Mozambique Basin: Implications for uplift history of the South African Plateau: Journal of African Earth Sciences, v. 109, p. 1–10, doi:10.1016/j.jafrearsci.2015.05.007.

Saria, E., Calais, E., Altamimi, Z., Willis, P., & Farah, H. (2013). A new velocity field for Africa from combined GPS and DORIS space geodetic solutions: contribution to the definition of the African reference frame (AFREF). Journal of Geophysical Research: Solid Earth, 118(4), 1677-1697.

Scholz, C. H., & Contreras, J. C. (1998). Mechanics of continental rift architecture. Geology, 26(11), 967-970.

Shillington, D.J., Accardo, N.J., Gallacher, R.J., Gaherty, J., Nyblade, A.A., and Mulibo, G., (2019), Kinematics of Active Deformation in the Malawi Rift and Rungwe Volcanic Province, Africa: Geochemistry, Geophysics, Geosystems, v. 20, p. 3928–3951, https://doi.org/10.1029/2019GC008354.

Specht, T. D., & Rosendahl, B. R. (1989). Architecture of the Lake Malawi Rift, East Africa. Journal of African Earth Sciences, 8(2–4), 355–382. https://doi.org/10.1016/S0899-5362(89)80032-6

Stamps, D. S., Calais, E., Saria, E., Hartnady, C., Nocquet, J. M., Ebinger, C. J., & Fernandes, R. M. (2008). A kinematic model for the East African Rift. Geophysical Research Letters, 35(5).

Stamps, D. S., Saria, E., & Kreemer, C. (2018). A geodetic strain rate model for the East African Rift System. Scientific reports, 8(1), 1-9.

Stamps, D. S., Kreemer, C., Fernandes, R., Rajaonarison, T. A., & Rambolamanana, G. (2021). Redefining East African Rift System kinematics. Geology, 49(2), 150-155.

Stockli D. F. (2005). Application of Low-Temperature Thermochronometry to Extensional Tectonic Settings. Reviews in Mineralogy and Geochemistry; 58 (1): 411–448. doi: https://doi.org/10.2138/rmg.2005.58.16

Thomson, S. N., Stöckhert, B., & Brix, M. R. (1998). Thermochronology of the high-pressure metamorphic rocks of Crete, Greece: Implications for the speed of tectonic processes.

Geology, 26(3), 259–262. https://doi.org/10.1130/0091-7613(1998)026<0259:TOTHPM>2.3.CO;2

Van der Beek, P., Mbede, E., Andriessen, P., & Delvaux, D. (1998). Denudation history of the Malawi and Rukwa Rift flanks (East African Rift system) from apatite fission track thermochronology. Journal of African Earth Sciences, 26(3), 363–385. https://doi.org/10.1016/S0899-5362(98)00021-9

Walford, H., White, N., and Sydow, J., 2005, Solid sediment load history of the Zambezi Delta: Earth and Planetary Science Letters, v. 238, p. 49–63, doi:10.1016/j.epsl.2005.07.014.

Wedmore, L. N., Biggs, J., Williams, J. N., Fagereng, Å., Dulanya, Z., Mphepo, F., & Mdala, H. (2020). Active fault scarps in southern Malawi and their implications for the distribution of strain in incipient continental rifts. Tectonics, 39(3), e2019TC005834.

Woldegabriel, G., Aronson, J. L., & Walter, R. C. (1990). Geology, geochronology, and rift basin development in the central sector of the Main Ethiopia Rift. Geological Society of America Bulletin, 102(4), 439-458.

WoldeGabriel, G., Olago, D., Dindi, E., & Owor, M. (2016). Genesis of the east African rift system. In Soda Lakes of East Africa (pp. 25-59). Springer, Cham.

Zanettin, B., EJ, V., & EM, P. (1979). Correlation Among Ethiopian Volcanic Formation with Special Reference to the Chronological and Stratigraphical Problems of the Trap Series.